

# Statistical higher-order multi-scale method for nonlinear thermo-mechanical simulation of random composite materials with temperature-dependent properties

Hao Dong<sup>a,\*</sup>, Junzhi Cui<sup>b</sup>

<sup>a</sup>*School of Mathematics and Statistics, Xidian University, Xi'an 710071, China*

<sup>b</sup>*Academy of Mathematics and Systems Science, Chinese Academy of Sciences, Beijing 100190, China.*

---

## Abstract

Stochastic multi-scale modeling and simulation for nonlinear thermo-mechanical problems of composite materials with complicated random microstructures remains a challenging issue. In this paper, we develop a novel statistical higher-order multi-scale (SHOMS) method for nonlinear thermo-mechanical simulation of random composite materials, which is designed to overcome limitations of prohibitive computation involving the macro-scale and micro-scale. By virtue of statistical multi-scale asymptotic analysis and Taylor series method, the SHOMS computational model is rigorously derived for accurately analyzing nonlinear thermo-mechanical responses of random composite materials both in the macro-scale and micro-scale. Moreover, the local error analysis of SHOMS solutions in the point-wise sense clearly illustrates the crucial indispensability of establishing the higher-order asymptotic corrected terms in SHOMS computational model for keeping the conservation of local energy and momentum. Then, the corresponding space-time multi-scale numerical algorithm with off-line and on-line stages is designed to efficiently simulate nonlinear thermo-mechanical behaviors of random composite materials. Finally, extensive numerical experiments are presented to gauge the efficiency and accuracy of the proposed SHOMS approach.

*Keywords:* random composite materials, nonlinear thermo-mechanical simulation, SHOMS computational model, space-time multi-scale algorithm, local error analysis

---

## 1. Introduction

In recent years, random composite materials have been extensively applied in a variety of engineering sectors, such as aviation, aerospace and civil construction, etc. By randomly distributing high-performance fibrous or particulate materials into ordinary matrix material, these synthetic composite materials exhibit high temperature resistance, high fatigue resistance and high fracture resistance, etc [1, 2]. Especially in aviation and aerospace industries, engineering structures manufactured by random composite materials often served under extreme heat environment while the thermal and mechanical properties of component materials exhibit significantly nonlinear temperature-dependent feature. These complicated nonlinear physical behaviors and randomly geometric heterogeneities of the considered structures raise a grand challenge for effective numerical simulation [3].

To the best of our knowledge, traditional numerical methods including the finite element method (FEM) [4, 5], boundary element method [6] and meshless method [7] have been adopted to the analysis and computation of nonlinear thermomechanical problems. Moreover, Abdoun et al. used homotopy and asymptotic numerical method to simulate and analyze the thermal buckling and vibration of laminated composite plates with temperature-dependent properties in [8]. In reference [9], Najibi et al. employed higher-order graded finite element method to conduct transient thermal stress analysis for a hollow FGM cylinder with nonlinear temperature-dependent material properties. In reference [10], the state space method and transfer-matrix method are adopted to obtain the displacements and stresses for the thick beams with temperature-dependent

---

\*Corresponding Author

Email address: donghaoxd@xidian.edu.cn (Hao Dong)

material properties under thermo-mechanical loads. However, it should be noted the equations, which govern the nonlinear thermo-mechanical behaviors for the composites, have rapidly varying and strongly discontinuous coefficients arising from the sharp variation between different constituents. As far as we know, the direct numerical simulation for composite materials needs a tremendous amount of computational resources or even ineffective to capture their microscopic behaviors due to the highly heterogeneous components.

To accomplish effective modeling and efficient simulation for inhomogeneous materials, scientists and engineers presented a variety of multi-scale methods, such as asymptotic homogenization method (AHM) [11], multi-scale finite element method (MsFEM) [12], heterogeneous multi-scale method (HMM) [13], variational multi-scale method (VMS) [14], multi-scale eigenelement method (MEM) [15], localized orthogonal decomposition method (LOD) [16] and finite volume based asymptotic homogenization theory (FVBAHT) [17], etc. However, numerical computation and theoretical analysis in [18, 19, 20] find that most of above-mentioned multi-scale methods are lower-order multi-scale method in essence, which can only capture macroscopic and inadequate microscopic information of heterogeneous materials, especially for high-contrast composite materials. To improve inadequate numerical accuracy of classical lower-order multi-scale approaches, Cui and his research team systematically developed a class of higher-order multi-scale methods, whose numerical accuracy is significantly improved for simulating authentic composite materials in practical engineering applications. Hence, these higher-order multi-scale approaches are extensively used in multi-physics coupling problems, stochastic multi-scale problem, structural mechanics problem and nonlinear multi-scale problem of heterogeneous materials, etc [21, 22, 23, 24, 25, 26, 27, 28]. The reviews of above-mentioned multi-scale approaches show that these methods have a strong potential to encourage important advances in modeling and simulating a certain range of composites' behaviors. However, they still need to be improved for composite materials with complex non-deterministic microstructure. The uncertainties in the microstructure prominently affect the mechanical properties of the composite materials. Some stochastic multi-scale computational schemes have been established in recent years based on perturbation-based stochastic finite element method [29, 30, 31], spectral stochastic finite element method [32, 33, 34] and stochastic collocation method [35, 36] for specific problems. Furthermore, combining with Monte Carlo method, the higher-order multi-scale methods proposed by Cui and his research team have been applied to simulate a wide range of physical behaviors of random composite materials [22, 23, 28, 37, 38, 39]. However, it is worth noting that there are few works about multi-scale thermo-mechanical simulation of random composite materials with temperature-dependent properties. Hence, it is of great theoretical and engineering values to develop effective multi-scale approaches for nonlinear thermo-mechanical simulation of random composite materials with temperature-dependent properties.

The reminder of our article is organized as follows: In Section 2 the investigated random nonlinear governing equations with initial-boundary conditions are herein introduced for describing heat conduction and mechanical deformation of random composites with temperature-dependent properties. Furthermore, stochastic multi-scale asymptotic analysis and Taylor expansion approach are employed to establish statistical higher-order multi-scale computational model for nonlinear thermo-mechanical simulation of random composites. Also, the local error analysis of SHOMS computational model are derived. In Section 3 we develop a space-time multi-scale numerical algorithm with off-line and on-line stages to efficiently simulate nonlinear thermo-mechanical behaviors of random composite materials. Illustrative examples are presented to validate the computational accuracy and efficiency of the proposed SHOMS computational model and corresponding numerical algorithm in Section 4. In the final section, we provide some meaningful conclusions and a brief outlook.

## 2. The establishment of statistical higher-order multi-scale computational model

### 2.1. Microscopic computer representation of random composite materials

In this study, the investigated composite materials are comprised of matrix and randomly distributed particles or fibers, as shown in Fig. 1.

Based on computer representation idea and its improved algorithm devised by Li, Cui and Dong [40, 41], we employ open-source Freefem++ software to establish the detailed computer representation algorithm for generating microscopic configurations of random composite materials as follows.

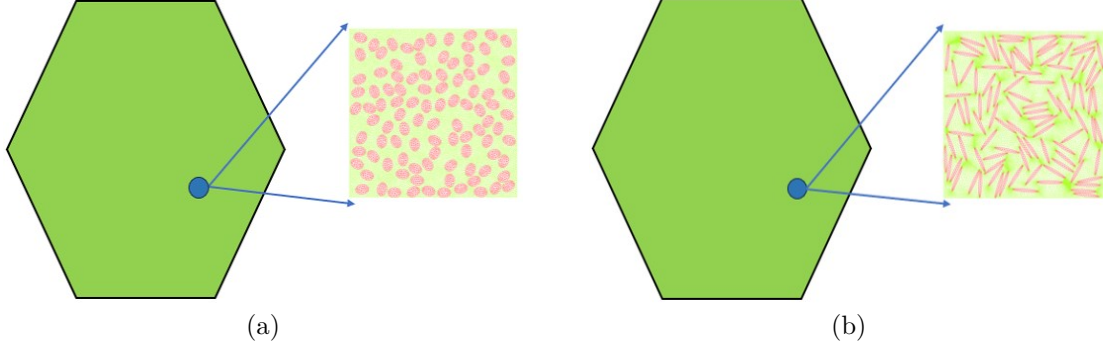


**Figure 1:** Random composite structures with different microscopic configurations. (a) Random particulate material; (b) Random fibrous material.

- (S1) Regarding random particulate and fibrous materials in Fig. 1(a) and Fig. 1(b), the probability distribution model is first employed to generate the random geometric parameters  $(x_1, x_2, a, b, \theta_1)$  or  $(x_1, x_2, x_3, a, b, c, \theta_1, \theta_2, \theta_3)$  of 2D or 3D randomly distributed configurations.
- (S2) Then, judge whether the newly generated configuration is located inside RVE and whether the newly generated configuration intersects with other previously generated configurations. For randomly distributed configurations, we use whether the distance between the centers of the previously generated configurations and newly generated configuration is greater than the sum of the radii of previously generated configurations and newly generated configuration as discriminate criterion. Additionally, to enhance the packing ratio of microscopic inclusions, we use whether there exist intersection points on previously generated configurations when connecting the centers of previously generated configurations and the points on the surface of newly generated configuration as revised discriminate criterion.
- (S3) When generating a sufficient amount of microscopic configurations, mesh generation algorithm based on Delaunay Refinement method (Freefem++ command: "buildmesh" or "tetg" for 2D or 3D geometrical configurations respectively) is adopted to create the microscopic configurations of the investigated random composites [42].

For geometric parameters  $(x_1, x_2, a, b, \theta_1)$  in 2D case,  $x_1$  and  $x_2$  represent the central coordinates of the elliptical inclusion for the  $x$ -axis and  $y$ -axis.  $a$  and  $b$  denote the lengths of the long half-axis and short half-axis of the elliptical inclusion and  $\theta_1$  represents the intersection angle between the long half-axis of the elliptical inclusion and the  $x$ -axis. For geometric parameters  $(x_1, x_2, x_3, a, b, c, \theta_1, \theta_2, \theta_3)$  in 3D case,  $x_1, x_2$  and  $x_3$  are the central coordinates of the ellipsoidal inclusion for the  $x$ -axis,  $y$ -axis and  $z$ -axis.  $a, b$  and  $c$  denote the lengths of the long half-axis, middle half-axis and short half-axis of the ellipsoidal inclusion.  $\theta_1, \theta_2$  and  $\theta_3$  are the three Euler angles of the ellipsoidal inclusion, respectively. Moreover, by elongating the elliptical or ellipsoidal particles and increasing the ratio of their long half-axis to short half-axis, the elliptical or ellipsoidal particles can be changed as fibrous inclusions. To sum up, the above-mentioned methodologies accomplish the effective generation of finite element mesh for random composites we investigated at micro-scale.

## 2.2. Setting of stochastic multi-scale nonlinear thermo-mechanical problems

The primary challenge for solving random multi-scale problems pertains to their auxiliary cell problems defined on the entire space  $\mathbb{R}^{\mathcal{N}} (\mathcal{N} = 2, 3)$ . To tackle this challenge, by using "periodization" and "cutoff" techniques in previous studies [22, 23, 28], the unit cell problems defined on an infinite domain are approximated by transforming them into unit cell problems on a finite domain with infinite random sampling, see Fig. 2 for a schematic explanation.

Based on the classical thermo-mechanical model [3], the stochastic governing equations for describing the nonlinear thermo-mechanical problems of random composite materials are reported, whose material

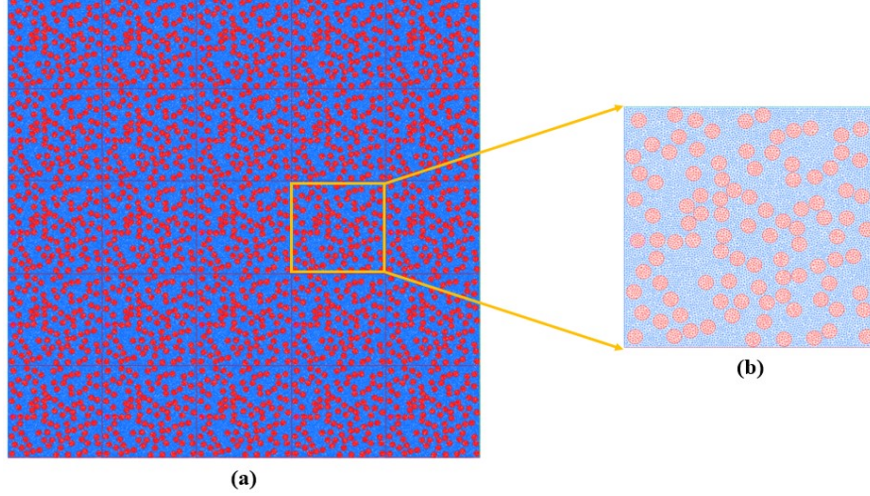


**Figure 2:** Random composite structures with a statistical periodic layout. (a) Macroscopic composite structure  $\Omega$ ; (b) Microscopic unit cell  $Y^s$ .

parameters all possess the temperature-dependent properties.

$$\begin{cases}
 \rho^\varepsilon(\mathbf{x}, T^\varepsilon, \boldsymbol{\omega}) c^\varepsilon(\mathbf{x}, T^\varepsilon, \boldsymbol{\omega}) \frac{\partial T^\varepsilon(\mathbf{x}, t, \boldsymbol{\omega})}{\partial t} - \frac{\partial}{\partial x_i} \left( k_{ij}^\varepsilon(\mathbf{x}, T^\varepsilon, \boldsymbol{\omega}) \frac{\partial T^\varepsilon(\mathbf{x}, t, \boldsymbol{\omega})}{\partial x_j} \right) = h(\mathbf{x}, t), & \text{in } \Omega \times (0, T^*), \\
 - \frac{\partial}{\partial x_j} \left( C_{ijkl}^\varepsilon(\mathbf{x}, T^\varepsilon, \boldsymbol{\omega}) \frac{\partial u_k^\varepsilon(\mathbf{x}, t, \boldsymbol{\omega})}{\partial x_l} - \beta_{ij}^\varepsilon(\mathbf{x}, T^\varepsilon, \boldsymbol{\omega}) (T^\varepsilon(\mathbf{x}, t, \boldsymbol{\omega}) - \tilde{T}) \right) = f_i(\mathbf{x}, t), & \text{in } \Omega \times (0, T^*), \\
 T^\varepsilon(\mathbf{x}, t, \boldsymbol{\omega}) = \hat{T}(\mathbf{x}, t), & \text{on } \partial\Omega_T \times (0, T^*), \\
 \mathbf{u}^\varepsilon(\mathbf{x}, t, \boldsymbol{\omega}) = \hat{\mathbf{u}}(\mathbf{x}, t), & \text{on } \partial\Omega_u \times (0, T^*), \\
 k_{ij}^\varepsilon(\mathbf{x}, T^\varepsilon, \boldsymbol{\omega}) \frac{\partial T^\varepsilon(\mathbf{x}, t, \boldsymbol{\omega})}{\partial x_j} n_i = \bar{q}(\mathbf{x}, t), & \text{on } \partial\Omega_q \times (0, T^*), \\
 [C_{ijkl}^\varepsilon(\mathbf{x}, T^\varepsilon, \boldsymbol{\omega}) \frac{\partial u_k^\varepsilon(\mathbf{x}, t, \boldsymbol{\omega})}{\partial x_l} - \beta_{ij}^\varepsilon(\mathbf{x}, T^\varepsilon, \boldsymbol{\omega}) (T^\varepsilon(\mathbf{x}, t, \boldsymbol{\omega}) - \tilde{T})] n_j = \bar{\sigma}_i(\mathbf{x}, t), & \text{on } \partial\Omega_\sigma \times (0, T^*), \\
 T^\varepsilon(\mathbf{x}, 0, \boldsymbol{\omega}) = \tilde{T}, & \text{in } \Omega.
 \end{cases} \quad (2.1)$$

Here,  $\Omega$  represents a bounded convex domain in  $\mathbb{R}^{\mathcal{N}}$  ( $\mathcal{N} = 2, 3$ ) with a boundary  $\partial\Omega$ . In the micro-scale, the domain  $\Omega$  can be defined by a statistical periodic layout of microscopic unit cell  $Y^s$  corresponding to random sample  $\omega^s$  ( $s = 1, 2, 3, \dots$  denotes the index of random samples), as shown in Fig. 2. The characteristic size of microscopic cell  $Y^s$  is characterized by a parameter  $\varepsilon$ . The  $u_i^\varepsilon(\mathbf{x}, t, \boldsymbol{\omega})$  and  $T^\varepsilon(\mathbf{x}, t, \boldsymbol{\omega})$  in equations (2.1) are the unresolved displacement and temperature fields.  $\rho^\varepsilon(\mathbf{x}, T^\varepsilon, \boldsymbol{\omega})$  is the mass density;  $c^\varepsilon(\mathbf{x}, T^\varepsilon, \boldsymbol{\omega})$  is specific heat;  $k_{ij}^\varepsilon(\mathbf{x}, T^\varepsilon, \boldsymbol{\omega})$  is the second order thermal conductivity tensor;  $C_{ijkl}^\varepsilon(\mathbf{x}, T^\varepsilon, \boldsymbol{\omega})$  is the fourth order elastic tensor;  $\beta_{ij}^\varepsilon(\mathbf{x}, T^\varepsilon, \boldsymbol{\omega})$  is the second order thermal modulus tensor. Furthermore, we assume that all material parameters satisfy Lipschitz continuous condition with respect to temperature variable  $T^\varepsilon$  and are statistical periodic functions [21].  $\hat{\mathbf{u}}(\mathbf{x}, t)$  is the prescribed displacements on the boundary  $\partial\Omega_u$ ,  $\hat{T}(\mathbf{x}, t)$  is the prescribed temperature on the boundary  $\partial\Omega_T$ ,  $\bar{\sigma}_i(\mathbf{x}, t)$  is the prescribed traction on the boundary  $\partial\Omega_\sigma$  with the normal vector  $n_j$ , and  $\bar{q}(\mathbf{x}, t)$  is the prescribed heat flux normal to the boundary  $\partial\Omega_q$  with the normal vector  $n_i$ ;  $\tilde{T}$  is the initial temperature when the composites are in stress-free state; The body forces and internal heat source are represented by  $f_i(\mathbf{x}, t)$  and  $h(\mathbf{x}, t)$ , respectively.

To begin with, let us set  $\mathbf{y} = \mathbf{x}/\varepsilon$  as microscopic coordinates of statistical periodic unit cell  $Y^s = (0, 1)^{\mathcal{N}}$ . With this notation, the material parameters  $\rho^\varepsilon(\mathbf{x}, T^\varepsilon, \boldsymbol{\omega})$ ,  $c^\varepsilon(\mathbf{x}, T^\varepsilon, \boldsymbol{\omega})$ ,  $k_{ij}^\varepsilon(\mathbf{x}, T^\varepsilon, \boldsymbol{\omega})$ ,  $C_{ijkl}^\varepsilon(\mathbf{x}, T^\varepsilon, \boldsymbol{\omega})$  and  $\beta_{ij}^\varepsilon(\mathbf{x}, T^\varepsilon, \boldsymbol{\omega})$  can be rewritten as  $\rho(\mathbf{y}, T^\varepsilon, \boldsymbol{\omega})$ ,  $c(\mathbf{y}, T^\varepsilon, \boldsymbol{\omega})$ ,  $k_{ij}(\mathbf{y}, T^\varepsilon, \boldsymbol{\omega})$ ,  $C_{ijkl}(\mathbf{y}, T^\varepsilon, \boldsymbol{\omega})$  and  $\beta_{ij}(\mathbf{y}, T^\varepsilon, \boldsymbol{\omega})$ .

Moreover, we have the chain rule for the performed spatial scales as follows.

$$\frac{\partial \Phi^\varepsilon(\mathbf{x}, t, \boldsymbol{\omega})}{\partial x_i} = \frac{\partial \Phi(\mathbf{x}, \mathbf{y}, t, \boldsymbol{\omega})}{\partial x_i} + \frac{1}{\varepsilon} \frac{\partial \Phi(\mathbf{x}, \mathbf{y}, t, \boldsymbol{\omega})}{\partial y_i}. \quad (2.2)$$

which will be extensively used in the sequel.

Moreover, in line with previous works such as [23, 24, 25, 26, 27], we make certain assumptions for the governing equations (2.1).

- (A)  $k_{ij}^\varepsilon(\mathbf{x}, T^\varepsilon, \boldsymbol{\omega})$ ,  $C_{ijkl}^\varepsilon(\mathbf{x}, T^\varepsilon, \boldsymbol{\omega})$  and  $\beta_{ij}^\varepsilon(\mathbf{x}, T^\varepsilon, \boldsymbol{\omega})$  are symmetric, and there exist two positive constant  $\gamma_0$  and  $\gamma_1$  independent of  $\varepsilon$  such that

$$\begin{aligned} k_{ij}^\varepsilon(\mathbf{x}, T^\varepsilon, \boldsymbol{\omega}) &= k_{ji}^\varepsilon(\mathbf{x}, T^\varepsilon, \boldsymbol{\omega}), \gamma_0 |\boldsymbol{\xi}|^2 \leq k_{ij}^\varepsilon(\mathbf{x}, T^\varepsilon, \boldsymbol{\omega}) \xi_i \xi_j \leq \gamma_1 |\boldsymbol{\xi}|^2, \\ C_{ijkl}^\varepsilon(\mathbf{x}, T^\varepsilon, \boldsymbol{\omega}) &= C_{ijlk}^\varepsilon(\mathbf{x}, T^\varepsilon, \boldsymbol{\omega}) = C_{klij}^\varepsilon(\mathbf{x}, T^\varepsilon, \boldsymbol{\omega}), \gamma_0 \eta_{ij} \eta_{kl} \leq C_{ijkl}^\varepsilon(\mathbf{x}, T^\varepsilon, \boldsymbol{\omega}) \eta_{ij} \eta_{kl} \leq \gamma_1 \eta_{ij} \eta_{kl}, \\ \beta_{ij}^\varepsilon(\mathbf{x}, T^\varepsilon, \boldsymbol{\omega}) &= \beta_{ji}^\varepsilon(\mathbf{x}, T^\varepsilon, \boldsymbol{\omega}), \gamma_0 |\boldsymbol{\xi}|^2 \leq \beta_{ij}^\varepsilon(\mathbf{x}, T^\varepsilon, \boldsymbol{\omega}) \xi_i \xi_j \leq \gamma_1 |\boldsymbol{\xi}|^2. \end{aligned}$$

where  $\{\eta_{ij}\}$  is an arbitrary symmetric matrix in  $R^{\mathcal{N} \times \mathcal{N}}$ ,  $\boldsymbol{\xi} = (\xi_1, \xi_2, \dots, \xi_{\mathcal{N}})$  is an arbitrary vector with real elements in  $R^{\mathcal{N}}$ , and  $(\mathbf{x}, T^\varepsilon)$  is an arbitrary point in  $\Omega \times [T_{min}, T_{max} + C_*]$ .

- (B)  $\rho^\varepsilon(\mathbf{x}, T^\varepsilon, \boldsymbol{\omega})$ ,  $c^\varepsilon(\mathbf{x}, T^\varepsilon, \boldsymbol{\omega})$ ,  $k_{ij}^\varepsilon(\mathbf{x}, T^\varepsilon, \boldsymbol{\omega})$ ,  $C_{ijkl}^\varepsilon(\mathbf{x}, T^\varepsilon, \boldsymbol{\omega})$  and  $\beta_{ij}^\varepsilon(\mathbf{x}, T^\varepsilon, \boldsymbol{\omega})$  are scalar functions belonging to  $L^\infty(\Omega)$ , and there are constants  $\rho^0$  and  $c^0$  such that

$$0 < \rho^0 \leq \rho^\varepsilon(\mathbf{x}, T^\varepsilon, \boldsymbol{\omega}), \quad 0 < c^0 \leq c^\varepsilon(\mathbf{x}, T^\varepsilon, \boldsymbol{\omega}).$$

functions  $\rho^\varepsilon(\mathbf{x}, T^\varepsilon, \boldsymbol{\omega})$ ,  $c^\varepsilon(\mathbf{x}, T^\varepsilon, \boldsymbol{\omega})$ ,  $k_{ij}^\varepsilon(\mathbf{x}, T^\varepsilon, \boldsymbol{\omega})$ ,  $C_{ijkl}^\varepsilon(\mathbf{x}, T^\varepsilon, \boldsymbol{\omega})$  and  $\beta_{ij}^\varepsilon(\mathbf{x}, T^\varepsilon, \boldsymbol{\omega})$  are 1-periodic of microscopic variable  $\mathbf{y}$  for stationary  $T^\varepsilon \in [T_{min}, T_{max} + C_*]$ .

- (C)  $h(\mathbf{x}, t) \in L^2(\Omega \times (0, T^*))$ ,  $f_i(\mathbf{x}, t) \in L^2(\Omega \times (0, T^*))$ ,  $\hat{T}(\mathbf{x}, t) \in L^2(0, T^*; H^1(\Omega))$ ,  $\hat{\mathbf{u}}(\mathbf{x}, t) \in L^2(0, T^*; H^1(\Omega))^3$ ,  $\bar{q}(\mathbf{x}, t) \in L^2(\Omega \times (0, T^*))$ ,  $\bar{\sigma}_i(\mathbf{x}, t) \in L^2(\Omega \times (0, T^*))$ .

### 2.3. Statistical higher-order multi-scale computational model of the governing equations

The proposed second-order two-scale computational model is established in this subsection. To the multi-scale problem (2.1), we suppose that  $T^\varepsilon(\mathbf{x}, t, \boldsymbol{\omega})$  and  $u_i^\varepsilon(\mathbf{x}, t, \boldsymbol{\omega})$  can be expanded as the following power series representations.

$$\begin{cases} T^\varepsilon(\mathbf{x}, t, \boldsymbol{\omega}) = T_0(\mathbf{x}, \mathbf{y}, t, \boldsymbol{\omega}) + \varepsilon T_1(\mathbf{x}, \mathbf{y}, t, \boldsymbol{\omega}) + \varepsilon^2 T_2(\mathbf{x}, \mathbf{y}, t, \boldsymbol{\omega}) + O(\varepsilon^3), \\ u_i^\varepsilon(\mathbf{x}, t, \boldsymbol{\omega}) = u_{i0}(\mathbf{x}, \mathbf{y}, t, \boldsymbol{\omega}) + \varepsilon u_{i1}(\mathbf{x}, \mathbf{y}, t, \boldsymbol{\omega}) + \varepsilon^2 u_{i2}(\mathbf{x}, \mathbf{y}, t, \boldsymbol{\omega}) + O(\varepsilon^3). \end{cases} \quad (2.3)$$

Below we focus on the implementation of solving the specific expanding forms of  $u_i^\varepsilon(\mathbf{x}, t, \boldsymbol{\omega})$  and  $T^\varepsilon(\mathbf{x}, t, \boldsymbol{\omega})$ . Firstly, the Taylor's formula of multivariate function is given as below [27]

$$f(x_0, y_0 + h, z_0) = f(x_0, y_0, z_0) + f_y(x_0, y_0, z_0)h + \frac{1}{2} f_{yy}(x_0, y_0, z_0)h^2 + O(h^3). \quad (2.4)$$

Then, the Taylor's formula (2.4) can be further rewritten by multi-index notation as follows [27]

$$f(x_0, y_0 + h, z_0) = f(x_0, y_0, z_0) + \mathbf{D}^{(0,1,0)} f(x_0, y_0, z_0)h + \frac{1}{2} \mathbf{D}^{(0,2,0)} f(x_0, y_0, z_0)h^2 + O(h^3). \quad (2.5)$$

By aid of the above-mentioned Taylor's formula (2.4) and multi-index notation (2.5), the material parameters

depending on temperature  $T^\varepsilon$  thus can be expanded as [27]

$$\begin{aligned}
k_{ij}^\varepsilon(\mathbf{x}, T^\varepsilon, \boldsymbol{\omega}) &= k_{ij}(\mathbf{y}, T^\varepsilon, \boldsymbol{\omega}) = C_{ijkl}(\mathbf{y}, T_0 + \varepsilon T_1 + \varepsilon^2 T_2 + O(\varepsilon^3), \boldsymbol{\omega}) \\
&= C_{ijkl}(\mathbf{y}, T_0, \boldsymbol{\omega}) + \mathbf{D}^{(0,1,0)} C_{ijkl}(\mathbf{y}, T_0, \boldsymbol{\omega}) [\varepsilon T_1 + \varepsilon^2 T_2 + O(\varepsilon^3)] \\
&\quad + \frac{1}{2} \mathbf{D}^{(0,2,0)} C_{ijkl}(\mathbf{y}, T_0, \boldsymbol{\omega}) [\varepsilon T_1 + \varepsilon^2 T_2 + O(\varepsilon^3)]^2 + O([\varepsilon T_1 + \varepsilon^2 T_2 + O(\varepsilon^3)]^3) \\
&= C_{ijkl}(\mathbf{y}, T_0, \boldsymbol{\omega}) + \varepsilon T_1 \mathbf{D}^{(0,1,0)} C_{ijkl}(\mathbf{y}, T_0, \boldsymbol{\omega}) \\
&\quad + \varepsilon^2 [T_2 \mathbf{D}^{(0,1,0)} C_{ijkl}(\mathbf{y}, T_0, \boldsymbol{\omega}) + \frac{1}{2} (T_1)^2 \mathbf{D}^{(0,2,0)} C_{ijkl}(\mathbf{y}, T_0, \boldsymbol{\omega})] + O(\varepsilon^3) \\
&= C_{ijkl}^{(0)} + \varepsilon C_{ijkl}^{(1)} + \varepsilon^2 C_{ijkl}^{(2)} + O(\varepsilon^3).
\end{aligned} \tag{2.6}$$

Using the similar expansion method as (2.6), other material parameters  $\rho^\varepsilon(\mathbf{x}, T^\varepsilon)$ ,  $c^\varepsilon(\mathbf{x}, T^\varepsilon)$ ,  $C_{ijkl}^\varepsilon(\mathbf{x}, T^\varepsilon)$  and  $\beta_{ij}^\varepsilon(\mathbf{x}, T^\varepsilon)$  are also expanded as the following forms

$$\begin{aligned}
\rho^\varepsilon(\mathbf{x}, T^\varepsilon, \boldsymbol{\omega}) &= \rho(\mathbf{y}, T_0, \boldsymbol{\omega}) + \varepsilon T_1 \mathbf{D}^{(0,1,0)} \rho(\mathbf{y}, T_0, \boldsymbol{\omega}) \\
&\quad + \varepsilon^2 [T_2 \mathbf{D}^{(0,1,0)} \rho(\mathbf{y}, T_0, \boldsymbol{\omega}) + \frac{1}{2} (T_1)^2 \mathbf{D}^{(0,2,0)} \rho(\mathbf{y}, T_0, \boldsymbol{\omega})] + O(\varepsilon^3) \\
&= \rho^{(0)} + \varepsilon \rho^{(1)} + \varepsilon^2 \rho^{(2)} + O(\varepsilon^3), \\
c^\varepsilon(\mathbf{x}, T^\varepsilon, \boldsymbol{\omega}) &= c(\mathbf{y}, T_0, \boldsymbol{\omega}) + \varepsilon T_1 \mathbf{D}^{(0,1,0)} c(\mathbf{y}, T_0, \boldsymbol{\omega}) \\
&\quad + \varepsilon^2 [T_2 \mathbf{D}^{(0,1,0)} c(\mathbf{y}, T_0, \boldsymbol{\omega}) + \frac{1}{2} (T_1)^2 \mathbf{D}^{(0,2,0)} c(\mathbf{y}, T_0, \boldsymbol{\omega})] + O(\varepsilon^3) \\
&= c^{(0)} + \varepsilon c^{(1)} + \varepsilon^2 c^{(2)} + O(\varepsilon^3), \\
C_{ijkl}^\varepsilon(\mathbf{x}, T^\varepsilon, \boldsymbol{\omega}) &= C_{ijkl}(\mathbf{y}, T_0, \boldsymbol{\omega}) + \varepsilon T_1 \mathbf{D}^{(0,1,0)} C_{ijkl}(\mathbf{y}, T_0, \boldsymbol{\omega}) \\
&\quad + \varepsilon^2 [T_2 \mathbf{D}^{(0,1,0)} C_{ijkl}(\mathbf{y}, T_0, \boldsymbol{\omega}) + \frac{1}{2} (T_1)^2 \mathbf{D}^{(0,2,0)} C_{ijkl}(\mathbf{y}, T_0, \boldsymbol{\omega}_{\mathbf{x}'})] + O(\varepsilon^3) \\
&= C_{ijkl}^{(0)} + \varepsilon C_{ijkl}^{(1)} + \varepsilon^2 C_{ijkl}^{(2)} + O(\varepsilon^3), \\
\beta_{ij}^\varepsilon(\mathbf{x}, T^\varepsilon, \boldsymbol{\omega}) &= \beta_{ij}(\mathbf{y}, T_0, \boldsymbol{\omega}) + \varepsilon T_1 \mathbf{D}^{(0,1,0)} \beta_{ij}(\mathbf{y}, T_0, \boldsymbol{\omega}) \\
&\quad + \varepsilon^2 [T_2 \mathbf{D}^{(0,1,0)} \beta_{ij}(\mathbf{y}, T_0, \boldsymbol{\omega}) + \frac{1}{2} (T_1)^2 \mathbf{D}^{(0,2,0)} \beta_{ij}(\mathbf{y}, T_0, \boldsymbol{\omega})] + O(\varepsilon^3) \\
&= \beta_{ij}^{(0)} + \varepsilon \beta_{ij}^{(1)} + \varepsilon^2 \beta_{ij}^{(2)} + O(\varepsilon^3).
\end{aligned} \tag{2.7}$$

By substituting equations (2.3), (2.6), and (2.7) into the multi-scale problem (2.1) and utilizing the chain rule (2.2), we can expand the derivatives and match terms with the same order of the small parameter  $\varepsilon$ .

This process allows us to reasonably obtain the following equations

$$\left\{ \begin{aligned} & \varepsilon^{-2} \frac{\partial}{\partial y_i} \left( k_{ij}^{(0)} \frac{\partial T_0}{\partial y_j} \right) + \varepsilon^{-1} \frac{\partial}{\partial y_i} \left( k_{ij}^{(1)} \frac{\partial T_0}{\partial y_j} \right) + \varepsilon^{-1} \frac{\partial}{\partial y_i} \left( k_{ij}^{(0)} \left( \frac{\partial T_0}{\partial x_j} + \frac{\partial T_1}{\partial y_j} \right) \right) \\ & + \varepsilon^{-1} \frac{\partial}{\partial x_i} \left( k_{ij}^{(0)} \frac{\partial T_0}{\partial y_j} \right) + \varepsilon^0 \frac{\partial}{\partial y_i} \left( k_{ij}^{(2)} \frac{\partial T_0}{\partial y_j} \right) + \varepsilon^0 \frac{\partial}{\partial x_i} \left( k_{ij}^{(1)} \frac{\partial T_0}{\partial y_j} \right) + \varepsilon^0 \frac{\partial}{\partial y_i} \left( k_{ij}^{(1)} \left( \frac{\partial T_0}{\partial x_j} + \frac{\partial T_1}{\partial y_j} \right) \right) \\ & + \varepsilon^0 \frac{\partial}{\partial y_i} \left( k_{ij}^{(0)} \left( \frac{\partial T_1}{\partial x_j} + \frac{\partial T_2}{\partial y_j} \right) \right) + \varepsilon^0 \frac{\partial}{\partial x_i} \left( k_{ij}^{(0)} \left( \frac{\partial T_0}{\partial x_j} + \frac{\partial T_1}{\partial y_j} \right) \right) + O(\varepsilon) = \varepsilon^0 \rho^{(0)} c^{(0)} \frac{\partial T_0}{\partial t} - h, \\ & \varepsilon^{-2} \frac{\partial}{\partial y_j} \left( C_{ijkl}^{(0)} \frac{\partial u_{k0}}{\partial y_l} \right) + \varepsilon^{-1} \frac{\partial}{\partial y_j} \left( C_{ijkl}^{(1)} \frac{\partial u_{k0}}{\partial y_l} \right) + \varepsilon^{-1} \frac{\partial}{\partial y_j} \left( C_{ijkl}^{(0)} \left( \frac{\partial u_{k0}}{\partial x_l} + \frac{\partial u_{k1}}{\partial y_l} \right) \right) \\ & + \varepsilon^{-1} \frac{\partial}{\partial x_j} \left( C_{ijkl}^{(0)} \frac{\partial u_{k0}}{\partial y_l} \right) - \varepsilon^{-1} \frac{\partial}{\partial y_j} \left( \beta_{ij}^{(0)} (T_0 - \tilde{T}) \right) + \varepsilon^0 \frac{\partial}{\partial y_j} \left( C_{ijkl}^{(2)} \frac{\partial u_{k0}}{\partial y_l} \right) \\ & + \varepsilon^0 \frac{\partial}{\partial y_j} \left( C_{ijkl}^{(1)} \left( \frac{\partial u_{k0}}{\partial x_l} + \frac{\partial u_{k1}}{\partial y_l} \right) \right) + \varepsilon^0 \frac{\partial}{\partial x_j} \left( C_{ijkl}^{(1)} \frac{\partial u_{k0}}{\partial y_l} \right) - \varepsilon^0 \frac{\partial}{\partial y_j} \left( \beta_{ij}^{(1)} (T_0 - \tilde{T}) \right) \\ & + \varepsilon^0 \frac{\partial}{\partial y_j} \left( C_{ijkl}^{(0)} \left( \frac{\partial u_{k1}}{\partial x_l} + \frac{\partial u_{k2}}{\partial y_l} \right) \right) - \varepsilon^0 \frac{\partial}{\partial x_j} \left( \beta_{ij}^{(0)} (T_0 - \tilde{T}) \right) \\ & - \varepsilon^0 \frac{\partial}{\partial y_j} \left( \beta_{ij}^{(0)} T_1 \right) + \varepsilon^0 \frac{\partial}{\partial x_j} \left( C_{ijkl}^{(0)} \left( \frac{\partial u_{k0}}{\partial x_l} + \frac{\partial u_{k1}}{\partial y_l} \right) \right) + O(\varepsilon) = -f_i. \end{aligned} \right. \quad (2.8)$$

As a consequence of equations (2.8), a series of equations are derived by matching terms of the same order of  $\varepsilon$ , following the classical procedure of AHM

$$O(\varepsilon^{-2}) : \left\{ \begin{aligned} & \frac{\partial}{\partial y_i} \left( k_{ij}^{(0)}(\mathbf{y}, T_0, \boldsymbol{\omega}) \frac{\partial T_0}{\partial y_j} \right) = 0, \\ & \frac{\partial}{\partial y_j} \left( C_{ijkl}^{(0)}(\mathbf{y}, T_0, \boldsymbol{\omega}) \frac{\partial u_{k0}}{\partial y_l} \right) = 0. \end{aligned} \right. \quad (2.9)$$

$$O(\varepsilon^{-1}) : \left\{ \begin{aligned} & \frac{\partial}{\partial y_i} \left( k_{ij}^{(1)}(\mathbf{y}, T_0, \boldsymbol{\omega}) \frac{\partial T_0}{\partial y_j} \right) + \frac{\partial}{\partial y_i} \left( k_{ij}^{(0)}(\mathbf{y}, T_0, \boldsymbol{\omega}) \left( \frac{\partial T_0}{\partial x_j} + \frac{\partial T_1}{\partial y_j} \right) \right) \\ & + \frac{\partial}{\partial x_i} \left( k_{ij}^{(0)}(\mathbf{y}, T_0, \boldsymbol{\omega}) \frac{\partial T_0}{\partial y_j} \right) = 0, \\ & \frac{\partial}{\partial y_j} \left( C_{ijkl}^{(1)}(\mathbf{y}, T_0, \boldsymbol{\omega}) \frac{\partial u_{k0}}{\partial y_l} \right) + \frac{\partial}{\partial y_j} \left( C_{ijkl}^{(0)}(\mathbf{y}, T_0, \boldsymbol{\omega}) \left( \frac{\partial u_{k0}}{\partial x_l} + \frac{\partial u_{k1}}{\partial y_l} \right) \right) \\ & + \frac{\partial}{\partial x_j} \left( C_{ijkl}^{(0)}(\mathbf{y}, T_0, \boldsymbol{\omega}) \frac{\partial u_{k0}}{\partial y_l} \right) - \frac{\partial}{\partial y_j} \left( \beta_{ij}^{(0)}(\mathbf{y}, T_0, \boldsymbol{\omega}) (T_0 - \tilde{T}) \right) = 0. \end{aligned} \right. \quad (2.10)$$

$$O(\varepsilon^0) : \left\{ \begin{aligned} & \frac{\partial}{\partial y_i} \left( k_{ij}^{(2)}(\mathbf{y}, T_0, \boldsymbol{\omega}) \frac{\partial T_0}{\partial y_j} \right) + \frac{\partial}{\partial x_i} \left( k_{ij}^{(1)}(\mathbf{y}, T_0, \boldsymbol{\omega}) \frac{\partial T_0}{\partial y_j} \right) \\ & + \frac{\partial}{\partial y_i} \left( k_{ij}^{(1)}(\mathbf{y}, T_0, \boldsymbol{\omega}) \left( \frac{\partial T_0}{\partial x_j} + \frac{\partial T_1}{\partial y_j} \right) \right) + \frac{\partial}{\partial y_i} \left( k_{ij}^{(0)}(\mathbf{y}, T_0, \boldsymbol{\omega}) \left( \frac{\partial T_1}{\partial x_j} + \frac{\partial T_2}{\partial y_j} \right) \right) \\ & + \frac{\partial}{\partial x_i} \left( k_{ij}^{(0)}(\mathbf{y}, T_0, \boldsymbol{\omega}) \left( \frac{\partial T_0}{\partial x_j} + \frac{\partial T_1}{\partial y_j} \right) \right) = \rho^{(0)}(\mathbf{y}, T_0, \boldsymbol{\omega}) c^{(0)}(\mathbf{y}, T_0, \boldsymbol{\omega}) \frac{\partial T_0}{\partial t} - h, \\ & \frac{\partial}{\partial y_j} \left( C_{ijkl}^{(2)}(\mathbf{y}, T_0, \boldsymbol{\omega}) \frac{\partial u_{k0}}{\partial y_l} \right) + \frac{\partial}{\partial y_j} \left( C_{ijkl}^{(1)}(\mathbf{y}, T_0, \boldsymbol{\omega}) \left( \frac{\partial u_{k0}}{\partial x_l} + \frac{\partial u_{k1}}{\partial y_l} \right) \right) \\ & + \frac{\partial}{\partial x_j} \left( C_{ijkl}^{(1)}(\mathbf{y}, T_0, \boldsymbol{\omega}) \frac{\partial u_{k0}}{\partial y_l} \right) - \frac{\partial}{\partial y_j} \left( \beta_{ij}^{(1)}(\mathbf{y}, T_0, \boldsymbol{\omega}) (T_0 - \tilde{T}) \right) \\ & + \frac{\partial}{\partial y_j} \left( C_{ijkl}^{(0)}(\mathbf{y}, T_0, \boldsymbol{\omega}) \left( \frac{\partial u_{k1}}{\partial x_l} + \frac{\partial u_{k2}}{\partial y_l} \right) \right) - \frac{\partial}{\partial x_j} \left( \beta_{ij}^{(0)}(\mathbf{y}, T_0, \boldsymbol{\omega}) (T_0 - \tilde{T}) \right) \\ & - \frac{\partial}{\partial y_j} \left( \beta_{ij}^{(0)}(\mathbf{y}, T_0, \boldsymbol{\omega}) T_1 \right) + \frac{\partial}{\partial x_j} \left( C_{ijkl}^{(0)}(\mathbf{y}, T_0, \boldsymbol{\omega}) \left( \frac{\partial u_{k0}}{\partial x_l} + \frac{\partial u_{k1}}{\partial y_l} \right) \right) = -f_i. \end{aligned} \right. \quad (2.11)$$

From (2.9), we next can determine that

$$T_0(\mathbf{x}, \mathbf{y}, t, \boldsymbol{\omega}) = T_0(\mathbf{x}, t), \quad u_{i0}(\mathbf{x}, \mathbf{y}, t, \boldsymbol{\omega}) = u_{i0}(\mathbf{x}, t). \quad (2.12)$$

Following this, taking advantage of (2.12), the terms  $\frac{\partial u_{k0}}{\partial y_l}$  and  $\frac{\partial T_0}{\partial y_j}$  both equate to zero. Subsequently, equations (2.10) can be further simplified as the subsequent equations.

$$\begin{cases} \frac{\partial}{\partial y_i} \left( k_{ij}^{(0)}(\mathbf{y}, T_0, \boldsymbol{\omega}) \frac{\partial T_1}{\partial y_j} \right) = - \frac{\partial}{\partial y_i} \left( k_{ij}^{(0)}(\mathbf{y}, T_0, \boldsymbol{\omega}) \frac{\partial T_0}{\partial x_j} \right), \\ \frac{\partial}{\partial y_j} \left( C_{ijkl}^{(0)}(\mathbf{y}, T_0, \boldsymbol{\omega}) \frac{\partial u_{k1}}{\partial y_l} \right) = - \frac{\partial}{\partial y_j} \left( C_{ijkl}^{(0)}(\mathbf{y}, T_0, \boldsymbol{\omega}) \frac{\partial u_{k0}}{\partial x_l} \right) + \frac{\partial}{\partial y_j} \left( \beta_{ij}^{(0)}(\mathbf{y}, T_0, \boldsymbol{\omega}) (T_0 - \tilde{T}) \right). \end{cases} \quad (2.13)$$

According to equations (2.13), we construct the separation forms of the first-order correctors  $u_{i1}$  and  $T_1$

$$\begin{cases} T_1(\mathbf{x}, \mathbf{y}, t, \boldsymbol{\omega}) = M_{\alpha_1}(\mathbf{y}, T_0, \boldsymbol{\omega}) \frac{\partial T_0}{\partial x_{\alpha_1}}, \\ u_{i1}(\mathbf{x}, \mathbf{y}, t, \boldsymbol{\omega}) = N_{im}^{\alpha_1}(\mathbf{y}, T_0, \boldsymbol{\omega}) \frac{\partial u_{m0}}{\partial x_{\alpha_1}} - P_i(\mathbf{y}, T_0, \boldsymbol{\omega}) (T_0 - \tilde{T}), \quad \alpha_1, \alpha_2, m, n = 1, 2, 3. \end{cases} \quad (2.14)$$

where  $M_{\alpha_1}$ ,  $N_{im}^{\alpha_1}$  and  $P_i$  are 1-periodic functions defined in microscopic unit cell  $Y^s$  for any random sample  $\boldsymbol{\omega}^s$ , which are defined as the first-order auxiliary cell functions. Now, substituting (2.14) into (2.13), the following equations with homogeneous Dirichlet boundary condition are obtained after simplification and calculation

$$\begin{cases} \frac{\partial}{\partial y_i} \left[ k_{ij}^{(0)}(\mathbf{y}, T_0, \boldsymbol{\omega}^s) \frac{\partial M_{\alpha_1}}{\partial y_j} \right] = - \frac{\partial k_{i\alpha_1}^{(0)}(\mathbf{y}, T_0, \boldsymbol{\omega}^s)}{\partial y_i}, & \mathbf{y} \in Y^s, \\ M_{\alpha_1}(\mathbf{y}, T_0, \boldsymbol{\omega}^s) = 0, & \mathbf{y} \in \partial Y^s. \end{cases} \quad (2.15)$$

$$\begin{cases} \frac{\partial}{\partial y_j} \left[ C_{ijkl}^{(0)}(\mathbf{y}, T_0, \boldsymbol{\omega}^s) \frac{\partial N_{km}^{\alpha_1}}{\partial y_l} \right] = - \frac{\partial C_{ijm\alpha_1}^{(0)}(\mathbf{y}, T_0, \boldsymbol{\omega}^s)}{\partial y_j}, & \mathbf{y} \in Y^s, \\ N_{km}^{\alpha_1}(\mathbf{y}, T_0, \boldsymbol{\omega}^s) = 0, & \mathbf{y} \in \partial Y^s. \end{cases} \quad (2.16)$$

$$\begin{cases} \frac{\partial}{\partial y_j} \left[ C_{ijkl}^{(0)}(\mathbf{y}, T_0, \boldsymbol{\omega}^s) \frac{\partial P_k}{\partial y_l} \right] = - \frac{\partial \beta_{ij}^{(0)}(\mathbf{y}, T_0, \boldsymbol{\omega}^s)}{\partial y_j}, & \mathbf{y} \in Y^s, \\ P_k(\mathbf{y}, T_0, \boldsymbol{\omega}^s) = 0, & \mathbf{y} \in \partial Y^s. \end{cases} \quad (2.17)$$

**Remark 1.** It should be mentioned that the first-order auxiliary cell functions are quasi-periodic functions which all depend on the expansion term  $T_0$ . Each expansion term  $T_0$  acts as a varying parameter. This is a significant difference compared to linear periodic composites.

Subsequently, we perform a volume integral on both sides of equations (2.11) on microscopic unit cell  $Y^s$  and apply the Gauss theorem on equations (2.11). By further applying the Kolmogorov's strong law of large numbers, these procedures allow to derive the macroscopic homogenized equations associated with

multi-scale problem (2.1) as presented below

$$\begin{cases} \hat{S}(T_0) \frac{\partial T_0}{\partial t} - \frac{\partial}{\partial x_i} \left( \hat{k}_{ij}(T_0) \frac{\partial T_0}{\partial x_j} \right) = h, & \text{in } \Omega \times (0, T^*), \\ - \frac{\partial}{\partial x_j} \left( \hat{C}_{ijkl}(T_0) \frac{\partial u_{k0}}{\partial x_l} - \hat{\beta}_{ij}(T_0)(T_0 - \tilde{T}) \right) = f_i, & \text{in } \Omega \times (0, T^*), \\ T_0(\mathbf{x}, t) = \hat{T}(\mathbf{x}, t), & \text{on } \partial\Omega_T \times (0, T^*), \\ \mathbf{u}_0(\mathbf{x}, t) = \hat{\mathbf{u}}(\mathbf{x}, t), & \text{on } \partial\Omega_u \times (0, T^*), \\ \hat{k}_{ij}(T_0) \frac{\partial T_0(\mathbf{x}, t)}{\partial x_j} n_i = \bar{q}(\mathbf{x}, t), & \text{on } \partial\Omega_q \times (0, T^*), \\ [\hat{C}_{ijkl}(T_0) \frac{\partial u_{k0}(\mathbf{x}, t)}{\partial x_l} - \hat{\beta}_{ij}(T_0)(T_0(\mathbf{x}, t) - \tilde{T})] n_j = \bar{\sigma}_i(\mathbf{x}, t), & \text{on } \partial\Omega_\sigma \times (0, T^*), \\ T_0(\mathbf{x}, 0) = \tilde{T}, & \text{in } \Omega. \end{cases} \quad (2.18)$$

Here, the macroscopic homogenized material parameters in (2.18) are defined as follows

$$\begin{aligned} \hat{S}(T_0) &= \lim_{M \rightarrow +\infty} \frac{\sum_{s=1}^M \hat{S}(T_0, \omega^s)}{M}, \\ \hat{k}_{ij}(T_0) &= \lim_{M \rightarrow +\infty} \frac{\sum_{s=1}^M \hat{k}_{ij}(T_0, \omega^s)}{M}, \\ \hat{C}_{ijkl}(T_0) &= \lim_{M \rightarrow +\infty} \frac{\sum_{s=1}^M \hat{C}_{ijkl}(T_0, \omega^s)}{M}, \\ \hat{\beta}_{ij}(T_0) &= \lim_{M \rightarrow +\infty} \frac{\sum_{s=1}^M \hat{\beta}_{ij}(T_0, \omega^s)}{M}, \end{aligned} \quad (2.19)$$

where the effective material coefficients in (2.19) are evaluated using the following formulas, which correspond to microscopic unit cell  $Y^s$  with random sample  $\omega^s$

$$\begin{aligned} \hat{S}(T_0, \omega^s) &= \frac{1}{|Y^s|} \int_{Y^s} \rho^{(0)}(\mathbf{y}, T_0, \omega^s) c^{(0)}(\mathbf{y}, T_0, \omega^s) dY^s, \\ \hat{k}_{ij}(T_0, \omega^s) &= \frac{1}{|Y^s|} \int_{Y^s} (k_{ij}^{(0)}(\mathbf{y}, T_0, \omega^s) + k_{ik}^{(0)}(\mathbf{y}, T_0, \omega^s) \frac{\partial M_j}{\partial y_k}) dY^s, \\ \hat{C}_{ijkl}(T_0, \omega^s) &= \frac{1}{|Y^s|} \int_{Y^s} (C_{ijkl}^{(0)}(\mathbf{y}, T_0, \omega^s) + C_{ijmn}^{(0)}(\mathbf{y}, T_0, \omega^s) \frac{\partial N_{mk}^l}{\partial y_n}) dY^s, \\ \hat{\beta}_{ij}(T_0, \omega^s) &= \frac{1}{|Y^s|} \int_{Y^s} (\beta_{ij}^{(0)}(\mathbf{y}, T_0, \omega^s) + C_{ijkl}^{(0)}(\mathbf{y}, T_0, \omega^s) \frac{\partial P_k}{\partial y_l}) dY^s. \end{aligned} \quad (2.20)$$

**Remark 2.** *It is important to emphasize that all homogenized material parameters vary with the macroscopic homogenized solution  $T_0$  due to the quasi-periodic properties of first-order cell functions. This discrepancy is significant when compared to linear composites.*

Now, we proceed to establish the vital second-order correctors  $u_{i2}$  and  $T_2$ . By substituting (2.12) and (2.14) into (2.11), and then subtracting (2.11) from (2.18), the following equations are obtained after simpli-

fication and computation

$$\left\{ \begin{aligned}
& \frac{\partial}{\partial y_i} \left( k_{ij}^{(0)}(\mathbf{y}, T_0, \boldsymbol{\omega}) \frac{\partial T_2}{\partial y_j} \right) = \left[ \rho^{(0)}(\mathbf{y}, T_0, \boldsymbol{\omega}) c^{(0)}(\mathbf{y}, T_0, \boldsymbol{\omega}) - \widehat{S}(T_0) \right] \frac{\partial T_0}{\partial t} \\
& + \left[ \widehat{k}_{\alpha_1 \alpha_2}(T_0) - k_{\alpha_1 \alpha_2}^{(0)}(\mathbf{y}, T_0, \boldsymbol{\omega}) - \frac{\partial}{\partial y_i} (k_{i \alpha_1}^{(0)}(\mathbf{y}, T_0, \boldsymbol{\omega}) M_{\alpha_2}) - k_{\alpha_1 j}(\mathbf{y}, T_0, \boldsymbol{\omega}) \frac{\partial M_{\alpha_2}}{\partial y_j} \right] \frac{\partial^2 T_0}{\partial x_{\alpha_1} \partial x_{\alpha_2}} \\
& + \left[ \frac{\partial \widehat{k}_{i \alpha_1}(T_0)}{\partial x_i} - \frac{\partial k_{i \alpha_1}^{(0)}(\mathbf{y}, T_0, \boldsymbol{\omega})}{\partial x_i} - \frac{\partial}{\partial y_i} (k_{ij}^{(0)}(\mathbf{y}, T_0, \boldsymbol{\omega}) \frac{\partial M_{\alpha_1}}{\partial x_j}) - \frac{\partial}{\partial x_i} (k_{ij}^{(0)}(\mathbf{y}, T_0, \boldsymbol{\omega}) \frac{\partial M_{\alpha_1}}{\partial y_j}) \right] \frac{\partial T_0}{\partial x_{\alpha_1}} \\
& - \frac{\partial}{\partial y_i} \left( M_{\alpha_1} \mathbf{D}^{(0,1)} k_{i \alpha_2}^{(0)}(\mathbf{y}, T_0, \boldsymbol{\omega}) + M_{\alpha_1} \mathbf{D}^{(0,1)} k_{ij}^{(0)}(\mathbf{y}, T_0, \boldsymbol{\omega}) \frac{\partial M_{\alpha_2}}{\partial y_j} \right) \frac{\partial T_0}{\partial x_{\alpha_1}} \frac{\partial T_0}{\partial x_{\alpha_2}}, \\
& \frac{\partial}{\partial y_j} \left( C_{ijkl}^{(0)}(\mathbf{y}, T_0, \boldsymbol{\omega}) \frac{\partial u_{k2}}{\partial y_l} \right) = \left[ \widehat{C}_{i \alpha_1 m \alpha_2}(T_0) - C_{i \alpha_1 m \alpha_2}^{(0)}(\mathbf{y}, T_0, \boldsymbol{\omega}) - \frac{\partial}{\partial y_j} (C_{ijk \alpha_1}^{(0)}(\mathbf{y}, T_0, \boldsymbol{\omega}) N_{km}^{\alpha_2}) \right. \\
& - C_{i \alpha_1 k j}^{(0)}(\mathbf{y}, T_0, \boldsymbol{\omega}) \frac{\partial N_{km}^{\alpha_2}}{\partial y_j} \left. \right] \frac{\partial^2 u_{m0}}{\partial x_{\alpha_1} \partial x_{\alpha_2}} + \left[ \frac{\partial \widehat{C}_{ij m \alpha_1}(T_0)}{\partial x_j} - \frac{\partial C_{ij m \alpha_1}^{(0)}(\mathbf{y}, T_0, \boldsymbol{\omega})}{\partial x_j} \right. \\
& - \frac{\partial}{\partial y_j} (C_{ijkl}^{(0)}(\mathbf{y}, T_0, \boldsymbol{\omega}) \frac{\partial N_{km}^{\alpha_1}}{\partial x_l}) - \frac{\partial}{\partial x_j} (C_{ijkl}^{(0)}(\mathbf{y}, T_0, \boldsymbol{\omega}) \frac{\partial N_{km}^{\alpha_1}}{\partial y_l}) \left. \right] \frac{\partial u_{m0}}{\partial x_{\alpha_1}} \\
& - \left[ \frac{\partial \widehat{\beta}_{ij}(T_0)}{\partial x_j} - \frac{\partial \beta_{ij}^{(0)}(\mathbf{y}, T_0, \boldsymbol{\omega})}{\partial x_j} - \frac{\partial}{\partial y_j} (C_{ijkl}^{(0)}(\mathbf{y}, T_0, \boldsymbol{\omega}) \frac{\partial P_k}{\partial x_l}) \right. \\
& - \frac{\partial}{\partial x_j} (C_{ijkl}^{(0)}(\mathbf{y}, T_0, \boldsymbol{\omega}) \frac{\partial P_k}{\partial y_l}) \left. \right] (T_0 - \widetilde{T}) - [\widehat{\beta}_{i \alpha_1}(T_0) - \beta_{i \alpha_1}^{(0)}(\mathbf{y}, T_0, \boldsymbol{\omega}) \\
& - C_{i \alpha_1 k l}^{(0)}(\mathbf{y}, T_0, \boldsymbol{\omega}) \frac{\partial P_k}{\partial y_l} - \frac{\partial}{\partial y_j} (C_{ijk \alpha_1}^{(0)}(\mathbf{y}, T_0, \boldsymbol{\omega}) P_k) - \frac{\partial}{\partial y_j} (\beta_{ij}^{(0)}(\mathbf{y}, T_0, \boldsymbol{\omega}) M_{\alpha_1})] \frac{\partial T_0}{\partial x_{\alpha_1}} \\
& + \frac{\partial}{\partial y_j} \left( M_{\alpha_1} \mathbf{D}^{(0,1)} \beta_{ij}^{(0)}(\mathbf{y}, T_0, \boldsymbol{\omega}) + M_{\alpha_1} \mathbf{D}^{(0,1)} C_{ijkl}^{(0)}(\mathbf{y}, T_0, \boldsymbol{\omega}) \frac{\partial P_k}{\partial y_l} \right) \frac{\partial T_0}{\partial x_{\alpha_1}} (T_0 - \widetilde{T}) \\
& - \frac{\partial}{\partial y_j} \left( M_{\alpha_1} \mathbf{D}^{(0,1)} C_{ij m \alpha_2}^{(0)}(\mathbf{y}, T_0, \boldsymbol{\omega}) + M_{\alpha_1} \mathbf{D}^{(0,1)} C_{ijkl}^{(0)}(\mathbf{y}, T_0, \boldsymbol{\omega}) \frac{\partial N_{km}^{\alpha_2}}{\partial y_l} \right) \frac{\partial T_0}{\partial x_{\alpha_1}} \frac{\partial u_{m0}}{\partial x_{\alpha_2}}.
\end{aligned} \right. \quad (2.21)$$

According to equations (2.20), then we construct the concrete expressions for  $u_{i2}$  and  $T_2$  as follows

$$\left\{ \begin{aligned}
& T_2(\mathbf{x}, \mathbf{y}, t, \boldsymbol{\omega}) = S(\mathbf{y}, T_0, \boldsymbol{\omega}) \frac{\partial T_0}{\partial t} + M_{\alpha_1 \alpha_2}(\mathbf{y}, T_0, \boldsymbol{\omega}) \frac{\partial^2 T_0}{\partial x_{\alpha_1} \partial x_{\alpha_2}} + R_{\alpha_1}(\mathbf{y}, T_0, \boldsymbol{\omega}) \frac{\partial T_0}{\partial x_{\alpha_1}} \\
& - B_{\alpha_1 \alpha_2}(\mathbf{y}, T_0, \boldsymbol{\omega}) \frac{\partial T_0}{\partial x_{\alpha_1}} \frac{\partial T_0}{\partial x_{\alpha_2}}, \\
& u_{i2}(\mathbf{x}, \mathbf{y}, t, \boldsymbol{\omega}) = N_{im}^{\alpha_1 \alpha_2}(\mathbf{y}, T_0, \boldsymbol{\omega}) \frac{\partial^2 u_{m0}}{\partial x_{\alpha_1} \partial x_{\alpha_2}} + Z_{im}^{\alpha_1}(\mathbf{y}, T_0, \boldsymbol{\omega}) \frac{\partial u_{m0}}{\partial x_{\alpha_1}} \\
& - Q_i(\mathbf{y}, T_0, \boldsymbol{\omega}) (T_0 - \widetilde{T}) - H_i^{\alpha_1}(\mathbf{y}, T_0, \boldsymbol{\omega}) \frac{\partial T_0}{\partial x_{\alpha_1}} \\
& + W_i^{\alpha_1}(\mathbf{y}, T_0, \boldsymbol{\omega}) \frac{\partial T_0}{\partial x_{\alpha_1}} (T_0 - \widetilde{T}) - A_{im}^{\alpha_1 \alpha_2}(\mathbf{y}, T_0, \boldsymbol{\omega}) \frac{\partial T_0}{\partial x_{\alpha_1}} \frac{\partial u_{m0}}{\partial x_{\alpha_2}}, \quad \alpha_1, \alpha_2, m, n = 1, 2, 3.
\end{aligned} \right. \quad (2.22)$$

In the above expressions,  $S$ ,  $M_{\alpha_1 \alpha_2}$ ,  $R_{\alpha_1}$ ,  $B_{\alpha_1 \alpha_2}$ ,  $N_{im}^{\alpha_1 \alpha_2}$ ,  $Z_{im}^{\alpha_1}$ ,  $Q_i$ ,  $H_i^{\alpha_1}$ ,  $W_i^{\alpha_1}$  and  $A_{im}^{\alpha_1 \alpha_2}$  are 1-periodic functions defined in microscopic unit cell  $Y^s$  for any random sample  $\boldsymbol{\omega}^s$ , which are referred to as second-order auxiliary cell functions. By substituting (2.21) into (2.20), a series of equations, which are attached with the homogeneous Dirichlet boundary condition, are derived as follows

$$\left\{ \begin{aligned}
& \frac{\partial}{\partial y_i} [k_{ij}^{(0)}(\mathbf{y}, T_0, \boldsymbol{\omega}^s) \frac{\partial S}{\partial y_j}] = \rho^{(0)} c^{(0)} - \widehat{S}, \quad \mathbf{y} \in Y^s, \\
& S(\mathbf{y}, T_0, \boldsymbol{\omega}^s) = 0, \quad \mathbf{y} \in \partial Y^s.
\end{aligned} \right. \quad (2.23)$$

$$\begin{cases} \frac{\partial}{\partial y_i} [k_{ij}^{(0)}(\mathbf{y}, T_0, \boldsymbol{\omega}^s) \frac{\partial M_{\alpha_1 \alpha_2}}{\partial y_j}] = \widehat{k}_{\alpha_1 \alpha_2} - k_{\alpha_1 \alpha_2}^{(0)} - \frac{\partial}{\partial y_i} (k_{i\alpha_1}^{(0)} M_{\alpha_2}) - k_{\alpha_1 j}^{(0)} \frac{\partial M_{\alpha_2}}{\partial y_j}, & \mathbf{y} \in Y^s, \\ M_{\alpha_1 \alpha_2}(\mathbf{y}, T_0, \boldsymbol{\omega}^s) = 0, & \mathbf{y} \in \partial Y^s. \end{cases} \quad (2.24)$$

$$\begin{cases} \frac{\partial}{\partial y_i} [k_{ij}^{(0)}(\mathbf{y}, T_0, \boldsymbol{\omega}^s) \frac{\partial R_{\alpha_1}}{\partial y_j}] = \frac{\partial \widehat{k}_{i\alpha_1}}{\partial x_i} - \frac{\partial k_{i\alpha_1}^{(0)}}{\partial x_i} - \frac{\partial}{\partial y_i} (k_{ij}^{(0)} \frac{\partial M_{\alpha_1}}{\partial x_j}) - \frac{\partial}{\partial x_i} (k_{ij}^{(0)} \frac{\partial M_{\alpha_1}}{\partial y_j}), & \mathbf{y} \in Y^s, \\ R_{\alpha_1}(\mathbf{y}, T_0, \boldsymbol{\omega}^s) = 0, & \mathbf{y} \in \partial Y^s. \end{cases} \quad (2.25)$$

$$\begin{cases} \frac{\partial}{\partial y_i} [k_{ij}^{(0)}(\mathbf{y}, T_0, \boldsymbol{\omega}^s) \frac{\partial B_{\alpha_1 \alpha_2}}{\partial y_j}] = \frac{\partial}{\partial y_i} (M_{\alpha_1} \mathbf{D}^{(0,1)} k_{i\alpha_2}^{(0)} + M_{\alpha_1} \mathbf{D}^{(0,1)} k_{ij}^{(0)} \frac{\partial M_{\alpha_2}}{\partial y_j}), & \mathbf{y} \in Y^s, \\ B_{\alpha_1 \alpha_2}(\mathbf{y}, T_0, \boldsymbol{\omega}^s) = 0, & \mathbf{y} \in \partial Y^s. \end{cases} \quad (2.26)$$

$$\begin{cases} \frac{\partial}{\partial y_j} [C_{ijkl}^{(0)}(\mathbf{y}, T_0, \boldsymbol{\omega}^s) \frac{\partial N_{km}^{\alpha_1 \alpha_2}}{\partial y_l}] = \widehat{C}_{i\alpha_1 m \alpha_2} - C_{i\alpha_1 m \alpha_2}^{(0)} \\ - \frac{\partial}{\partial y_j} (C_{ijk\alpha_1}^{(0)} N_{km}^{\alpha_2}) - C_{i\alpha_1 k j}^{(0)} \frac{\partial N_{km}^{\alpha_2}}{\partial y_j}, & \mathbf{y} \in Y^s, \\ N_{km}^{\alpha_1 \alpha_2}(\mathbf{y}, T_0, \boldsymbol{\omega}^s) = 0, & \mathbf{y} \in \partial Y^s. \end{cases} \quad (2.27)$$

$$\begin{cases} \frac{\partial}{\partial y_j} [C_{ijkl}^{(0)}(\mathbf{y}, T_0, \boldsymbol{\omega}^s) \frac{\partial Z_{km}^{\alpha_1}}{\partial y_l}] = \frac{\partial \widehat{C}_{ijm\alpha_1}}{\partial x_j} - \frac{\partial C_{ijm\alpha_1}^{(0)}}{\partial x_j} \\ - \frac{\partial}{\partial y_j} (C_{ijk l}^{(0)} \frac{\partial N_{km}^{\alpha_1}}{\partial x_l}) - \frac{\partial}{\partial x_j} (C_{ijkl}^{(0)} \frac{\partial N_{km}^{\alpha_1}}{\partial y_l}), & \mathbf{y} \in Y^s, \\ Z_{km}^{\alpha_1}(\mathbf{y}, T_0, \boldsymbol{\omega}^s) = 0, & \mathbf{y} \in \partial Y^s. \end{cases} \quad (2.28)$$

$$\begin{cases} \frac{\partial}{\partial y_j} [C_{ijkl}^{(0)}(\mathbf{y}, T_0, \boldsymbol{\omega}^s) \frac{\partial Q_k}{\partial y_l}] = \frac{\partial \widehat{\beta}_{ij}}{\partial x_j} - \frac{\partial \beta_{ij}^{(0)}}{\partial x_j} - \frac{\partial}{\partial y_j} (C_{ijkl}^{(0)} \frac{\partial P_k}{\partial x_l}) - \frac{\partial}{\partial x_j} (C_{ijkl}^{(0)} \frac{\partial P_k}{\partial y_l}), & \mathbf{y} \in Y^s, \\ Q_k(\mathbf{y}, T_0, \boldsymbol{\omega}^s) = 0, & \mathbf{y} \in \partial Y^s. \end{cases} \quad (2.29)$$

$$\begin{cases} \frac{\partial}{\partial y_j} [C_{ijkl}^{(0)}(\mathbf{y}, T_0, \boldsymbol{\omega}^s) \frac{\partial H_k^{\alpha_1}}{\partial y_l}] = \widehat{\beta}_{i\alpha_1} - \beta_{i\alpha_1}^{(0)} - C_{i\alpha_1 k l}^{(0)} \frac{\partial P_k}{\partial y_l} \\ - \frac{\partial}{\partial y_j} (C_{ijk\alpha_1}^{(0)} P_k) - \frac{\partial}{\partial y_j} (\beta_{ij}^{(0)} M_{\alpha_1}), & \mathbf{y} \in Y^s, \\ H_k^{\alpha_1}(\mathbf{y}, T_0, \boldsymbol{\omega}^s) = 0, & \mathbf{y} \in \partial Y^s. \end{cases} \quad (2.30)$$

$$\begin{cases} \frac{\partial}{\partial y_j} [C_{ijkl}^{(0)}(\mathbf{y}, T_0, \boldsymbol{\omega}^s) \frac{\partial W_k^{\alpha_1}}{\partial y_l}] = \frac{\partial}{\partial y_j} (M_{\alpha_1} \mathbf{D}^{(0,1)} \beta_{ij}^{(0)} + M_{\alpha_1} \mathbf{D}^{(0,1)} C_{ijkl}^{(0)} \frac{\partial P_k}{\partial y_l}), & \mathbf{y} \in Y^s, \\ W_k^{\alpha_1}(\mathbf{y}, T_0, \boldsymbol{\omega}^s) = 0, & \mathbf{y} \in \partial Y^s. \end{cases} \quad (2.31)$$

$$\begin{cases} \frac{\partial}{\partial y_j} [C_{ijkl}^{(0)}(\mathbf{y}, T_0, \boldsymbol{\omega}^s) \frac{\partial A_{km}^{\alpha_1 \alpha_2}}{\partial y_l}] = \frac{\partial}{\partial y_j} (M_{\alpha_1} \mathbf{D}^{(0,1)} C_{ijm\alpha_2}^{(0)} + M_{\alpha_1} \mathbf{D}^{(0,1)} C_{ijkl}^{(0)} \frac{\partial N_{km}^{\alpha_2}}{\partial y_l}), & \mathbf{y} \in Y^s, \\ A_{km}^{\alpha_1 \alpha_2}(\mathbf{y}, T_0, \boldsymbol{\omega}^s) = 0, & \mathbf{y} \in \partial Y^s. \end{cases} \quad (2.32)$$

Summing up, the macro-micro coupled SHOMS asymptotic solutions of the multi-scale nonlinear dynamic thermo-mechanical problem (2.1) are established as follows

$$\begin{aligned} \widehat{T}^\varepsilon(\mathbf{x}, t, \boldsymbol{\omega}) &= T_0(\mathbf{x}, t) + \varepsilon M_{\alpha_1}(\mathbf{y}, T_0, \boldsymbol{\omega}) \frac{\partial T_0(\mathbf{x}, t)}{\partial x_{\alpha_1}} \\ &\quad + \varepsilon^2 [S(\mathbf{y}, T_0, \boldsymbol{\omega}) \frac{\partial T_0(\mathbf{x}, t)}{\partial t} + M_{\alpha_1 \alpha_2}(\mathbf{y}, T_0, \boldsymbol{\omega}) \frac{\partial^2 T_0(\mathbf{x}, t)}{\partial x_{\alpha_1} \partial x_{\alpha_2}} \\ &\quad + R_{\alpha_1}(\mathbf{y}, T_0, \boldsymbol{\omega}) \frac{\partial T_0(\mathbf{x}, t)}{\partial x_{\alpha_1}} - B_{\alpha_1 \alpha_2}(\mathbf{y}, T_0, \boldsymbol{\omega}) \frac{\partial T_0(\mathbf{x}, t)}{\partial x_{\alpha_1}} \frac{\partial T_0(\mathbf{x}, t)}{\partial x_{\alpha_2}}]. \end{aligned} \quad (2.33)$$

$$\begin{aligned}
\hat{u}_i^\varepsilon(\mathbf{x}, t, \boldsymbol{\omega}) &= u_{i0}(\mathbf{x}, t) + \varepsilon \left[ N_{im}^{\alpha_1}(\mathbf{y}, T_0, \boldsymbol{\omega}) \frac{\partial u_{m0}(\mathbf{x}, t)}{\partial x_{\alpha_1}} - P_i(\mathbf{y}, T_0, \boldsymbol{\omega})(T_0(\mathbf{x}, t) - \tilde{T}) \right] \\
&+ \varepsilon^2 \left[ N_{im}^{\alpha_1 \alpha_2}(\mathbf{y}, T_0, \boldsymbol{\omega}) \frac{\partial^2 u_{m0}(\mathbf{x}, t)}{\partial x_{\alpha_1} \partial x_{\alpha_2}} + Z_{im}^{\alpha_1}(\mathbf{y}, T_0, \boldsymbol{\omega}) \frac{\partial u_{m0}(\mathbf{x}, t)}{\partial x_{\alpha_1}} \right. \\
&- Q_i(\mathbf{y}, T_0, \boldsymbol{\omega})(T_0(\mathbf{x}, t) - \tilde{T}) - H_i^{\alpha_1}(\mathbf{y}, T_0, \boldsymbol{\omega}) \frac{\partial T_0(\mathbf{x}, t)}{\partial x_{\alpha_1}} \\
&\left. + W_i^{\alpha_1}(\mathbf{y}, T_0, \boldsymbol{\omega}) \frac{\partial T_0(\mathbf{x}, t)}{\partial x_{\alpha_1}} (T_0(\mathbf{x}, t) - \tilde{T}) - A_{im}^{\alpha_1 \alpha_2}(\mathbf{y}, T_0, \boldsymbol{\omega}) \frac{\partial T_0(\mathbf{x}, t)}{\partial x_{\alpha_1}} \frac{\partial u_{m0}(\mathbf{x}, t)}{\partial x_{\alpha_2}} \right].
\end{aligned} \tag{2.34}$$

**Remark 3.** It is worth emphasizing that the proposed macro-micro coupled SHOMS asymptotic solutions of the multi-scale nonlinear dynamic thermo-mechanical problem (2.1) can be reasonably degenerated to the SHOMS asymptotic solutions of the multi-scale linear dynamic thermo-mechanical problem. Since the material parameters of multi-scale linear dynamic thermo-mechanical problem are independent with temperature variable  $T^\varepsilon$ , the second-order cell functions  $R_{\alpha_1}$ ,  $B_{\alpha_1 \alpha_2}$ ,  $Z_{im}^{\alpha_1}$ ,  $Q_i$ ,  $W_i^{\alpha_1}$  and  $A_{im}^{\alpha_1 \alpha_2}$  will be degenerated to zero and disappear in formulas (2.34) and (2.35).

Based on the theoretical analysis mentioned above, the macro-micro coupled SHOMS computational model has been established. This computational model includes first-order and second-order auxiliary cell model in micro-scale, homogenized model in macro-scale and macro-micro coupled SHOMS solutions. Furthermore, by respecting the chain rule (2.2) and the macro-micro asymptotic formulas (2.34) and (2.35), the heat fluxes, strains and stresses and inside  $\Omega$  of random composite materials with temperature-dependent properties are approximately evaluated as follows

$$\hat{q}_i^\varepsilon(\mathbf{x}, t, \boldsymbol{\omega}) = -k_{ij}^\varepsilon(\mathbf{x}, T^\varepsilon, \boldsymbol{\omega}) \frac{\partial \hat{T}^\varepsilon(\mathbf{x}, t, \boldsymbol{\omega})}{\partial x_j}. \tag{2.35}$$

$$\hat{\varepsilon}_{ij}^\varepsilon(\mathbf{x}, t, \boldsymbol{\omega}) = \frac{1}{2} \left[ \frac{\partial \hat{u}_i^\varepsilon(\mathbf{x}, t, \boldsymbol{\omega})}{\partial x_j} + \frac{\partial \hat{u}_j^\varepsilon(\mathbf{x}, t, \boldsymbol{\omega})}{\partial x_i} \right]. \tag{2.36}$$

and

$$\hat{\sigma}_{ij}^\varepsilon(\mathbf{x}, t, \boldsymbol{\omega}) = C_{ijkl}^\varepsilon(\mathbf{x}, T^\varepsilon, \boldsymbol{\omega}) \frac{\partial \hat{u}_k^\varepsilon(\mathbf{x}, t, \boldsymbol{\omega})}{\partial x_l} - \beta_{ij}^\varepsilon(\mathbf{x}, T^\varepsilon, \boldsymbol{\omega})(\hat{T}^\varepsilon(\mathbf{x}, t, \boldsymbol{\omega}) - \tilde{T}). \tag{2.37}$$

#### 2.4. Local error analysis of statistical multi-scale solutions in point-wise sense

In this subsection, we begin by introducing the multi-scale approximate solutions of stochastic multi-scale problem (2.1) as follows

$$\begin{aligned}
T^{(1\varepsilon)}(\mathbf{x}, t, \boldsymbol{\omega}) &= T_0 + \varepsilon T_1, \quad u_i^{(1\varepsilon)}(\mathbf{x}, t, \boldsymbol{\omega}) = u_{i0} + \varepsilon u_{i1}, \\
T^{(2\varepsilon)}(\mathbf{x}, t, \boldsymbol{\omega}) &= T_0 + \varepsilon T_1 + \varepsilon^2 T_2, \quad u_i^{(2\varepsilon)}(\mathbf{x}, t, \boldsymbol{\omega}) = u_{i0} + \varepsilon u_{i1} + \varepsilon^2 u_{i2},
\end{aligned} \tag{2.38}$$

where we defined  $T_0$  and  $u_{i0}$  as the macroscopic homogenized solutions,  $T^{(1\varepsilon)}$  and  $u_i^{(1\varepsilon)}$  as the statistical lower-order multi-scale (SLOMS) solutions,  $T^{(2\varepsilon)}$  and  $u_i^{(2\varepsilon)}$  as the SHOMS approximate solutions, which equate to  $\hat{T}^\varepsilon$  in (2.33) and  $\hat{u}_i^\varepsilon$  in (2.34), respectively.

Next, we introduce the following residual functions for the purpose of numerical accuracy analysis.

$$\begin{aligned}
T_{\Delta}^{(1\varepsilon)}(\mathbf{x}, t, \boldsymbol{\omega}) &= T^\varepsilon - T^{(1\varepsilon)}, \quad u_{\Delta i}^{(1\varepsilon)}(\mathbf{x}, t, \boldsymbol{\omega}) = u_i^\varepsilon - u_i^{(1\varepsilon)}, \\
T_{\Delta}^{(2\varepsilon)}(\mathbf{x}, t, \boldsymbol{\omega}) &= T^\varepsilon - T^{(2\varepsilon)}, \quad u_{\Delta i}^{(2\varepsilon)}(\mathbf{x}, t, \boldsymbol{\omega}) = u_i^\varepsilon - u_i^{(2\varepsilon)}.
\end{aligned} \tag{2.39}$$

After that, by inserting  $T_{\Delta}^{(1\varepsilon)}$  and  $u_{\Delta i}^{(1\varepsilon)}$  from (2.39) into (2.1), the following residual equations of SLOMS

solutions are obtained, which hold in the distribution sense.

$$\left\{ \begin{array}{l} \rho^\varepsilon(\mathbf{x}, T^\varepsilon, \boldsymbol{\omega}) c^\varepsilon(\mathbf{x}, T^\varepsilon, \boldsymbol{\omega}) \frac{\partial T_\Delta^{(1\varepsilon)}}{\partial t} - \frac{\partial}{\partial x_i} \left( k_{ij}^\varepsilon(\mathbf{x}, T^\varepsilon, \boldsymbol{\omega}) \frac{\partial T_\Delta^{(1\varepsilon)}}{\partial x_j} \right) \\ \quad = \mathbb{F}_0(\mathbf{x}, \mathbf{y}, t, \boldsymbol{\omega}) + \varepsilon \mathbb{F}_1(\mathbf{x}, \mathbf{y}, t, \boldsymbol{\omega}), \quad \text{in } \Omega \times (0, T^*), \\ - \frac{\partial}{\partial x_j} \left( C_{ijkl}^\varepsilon(\mathbf{x}, T^\varepsilon, \boldsymbol{\omega}) \frac{\partial u_{\Delta k}^{(1\varepsilon)}}{\partial x_l} - \beta_{ij}^\varepsilon(\mathbf{x}, T^\varepsilon, \boldsymbol{\omega}) (T_\Delta^{(1\varepsilon)} - \tilde{T}) \right) \\ \quad = \mathbb{S}_{0i}(\mathbf{x}, \mathbf{y}, t, \boldsymbol{\omega}) + \varepsilon \mathbb{S}_{1i}(\mathbf{x}, \mathbf{y}, t, \boldsymbol{\omega}), \quad \text{in } \Omega \times (0, T^*). \end{array} \right. \quad (2.40)$$

Here, the detailed forms of  $\mathbb{S}_{0i}(\mathbf{x}, \mathbf{y}, t, \boldsymbol{\omega})$ ,  $\mathbb{S}_{1i}(\mathbf{x}, \mathbf{y}, t, \boldsymbol{\omega})$ ,  $\mathbb{F}_0(\mathbf{x}, \mathbf{y}, t, \boldsymbol{\omega})$  and  $\mathbb{F}_1(\mathbf{x}, \mathbf{y}, t, \boldsymbol{\omega})$  can be obtained easily by referring to the results in [27]. However, due to their lengthy expressions, they are not exhibited in the current study.

Furthermore, by substituting  $T_\Delta^{(2\varepsilon)}$  and  $u_{\Delta i}^{(2\varepsilon)}$  from (2.39) into (2.1), the resulting residual equations of SHOMS solutions are derived, which also hold in the distribution sense.

$$\left\{ \begin{array}{l} \rho^\varepsilon(\mathbf{x}, T^\varepsilon, \boldsymbol{\omega}) c^\varepsilon(\mathbf{x}, T^\varepsilon, \boldsymbol{\omega}) \frac{\partial T_\Delta^{(2\varepsilon)}}{\partial t} - \frac{\partial}{\partial x_i} \left( k_{ij}^\varepsilon(\mathbf{x}, T^\varepsilon, \boldsymbol{\omega}) \frac{\partial T_\Delta^{(2\varepsilon)}}{\partial x_j} \right) \\ \quad = \varepsilon \mathbb{G}(\mathbf{x}, \mathbf{y}, t, \boldsymbol{\omega}), \quad \text{in } \Omega \times (0, T^*), \\ - \frac{\partial}{\partial x_j} \left( C_{ijkl}^\varepsilon(\mathbf{x}, T^\varepsilon, \boldsymbol{\omega}) \frac{\partial u_{\Delta k}^{(2\varepsilon)}}{\partial x_l} - \beta_{ij}^\varepsilon(\mathbf{x}, T^\varepsilon, \boldsymbol{\omega}) (T_\Delta^{(2\varepsilon)} - \tilde{T}) \right) \\ \quad = \varepsilon \mathbb{H}_i(\mathbf{x}, \mathbf{y}, t, \boldsymbol{\omega}), \quad \text{in } \Omega \times (0, T^*). \end{array} \right. \quad (2.41)$$

In the above residual equations, the specific forms of  $\mathbb{H}_i(\mathbf{x}, \mathbf{y}, t, \boldsymbol{\omega})$  and  $\mathbb{G}(\mathbf{x}, \mathbf{y}, t, \boldsymbol{\omega})$  are also not displayed in the present study owing to the same reason mentioned above.

In conclusion, the numerical accuracy analysis in the point-wise sense is presented, focusing on the residual equations (2.40) and (2.41). Noting the residual equations (2.40), it can be concluded that the residual error of SLOMS solutions is of order- $O(1)$  in the point-wise sense, primarily due to the presence of terms  $\mathbb{S}_{0i}(\mathbf{x}, \mathbf{y}, t, \boldsymbol{\omega})$  and  $\mathbb{F}_0(\mathbf{x}, \mathbf{y}, t, \boldsymbol{\omega})$ . Comparing with the residual equations (2.41), the residual error of SHOMS solutions is of order- $O(\varepsilon)$  in the point-wise sense. This implies that the SHOMS solutions can satisfy the local energy conservation of thermal equation and local momentum conservation of mechanical equations of the original stochastic multi-scale equations (2.1) in the point-wise sense. Thus even  $\varepsilon$  is a small constant, the SHOMS solutions can still provide the required accuracy for engineering computation and accurately capture the microscopic oscillating behaviors exhibited by random composite materials. This is the fundamental rationale and motivation for us to establish higher-order corrected terms and develop the SHOMS solutions.

### 3. Space-time multi-scale numerical algorithm

In this section, an innovative space-time multi-scale numerical algorithm with off-line and on-line stages is presented for the stochastic nonlinear governing equations (2.1), which is based on the FEM in spatial region and the finite difference method (FDM) in time direction. The detailed algorithm procedures for stochastic multi-scale nonlinear problem (2.1) are listed as follows.

#### 3.1. Off-line computation for microscopic cell problems

- (1) Generate a random sample  $\omega^s$  for microscopic unit cell  $Y^s$  according to a given probability distribution model  $\bar{P}$  and the volume fractions. And then, partition  $Y^s$  into finite element meshes  $J^{h_1} = \{K\}$  where  $h_1 = \max_K \{h_K\}$  and define the linear conforming finite element space  $V_{h_1}(Y^s) = \{\nu \in C^0(\bar{Y}^s) : \nu|_{\partial Y^s} = 0, \nu|_K \in P_1(K)\} \subset H_0^1(Y^s)$ .
- (2) Define service temperature range  $[T_{min}, T_{max}]$  of investigated random composite materials and choose a certain number of representative macroscopic parameters  $\bar{T}_s$  in service temperature range where  $s = 1, 2, \dots, \bar{L} (\bar{L} \in \mathbf{N}^*)$ . Then, solve the first-order auxiliary cell problems (2.15)-(2.17) with given material

properties on  $V_{h_1}(Y^s)$  corresponding to distinct representative macroscopic parameters  $\bar{T}_s$ . The specific FEM scheme for auxiliary cell problem (2.15) is established as follows

$$\int_{Y^s} k_{ij}^{(0)}(\mathbf{y}, T_0, \omega^s) \frac{\partial H_{\alpha_1}(\mathbf{y}, T_0, \omega^s)}{\partial y_j} \frac{\partial v^{h_1}}{\partial y_i} dY^s = - \int_{Y^s} k_{i\alpha_1}^{(0)}(\mathbf{y}, T_0, \omega^s) \frac{\partial v^{h_1}}{\partial y_i} dY^s, \quad \forall v^{h_1} \in V_{h_1}(Y^s). \quad (3.42)$$

Other first-order auxiliary cell problems can be solved similarly.

- (3) Repeat Steps 1 and 2 for different random samples  $\omega^s$  ( $s = 1, \dots, M$ ) and compute macroscopic homogenized material parameters  $\hat{S}(T_0)$ ,  $\hat{k}_{ij}(T_0)$ ,  $\hat{C}_{ijkl}(T_0)$  and  $\hat{\beta}_{ij}(T_0)$  by using the formula (2.19) corresponding to different macroscopic parameters  $\bar{T}_s$ .
- (4) Employing the same mesh as first-order auxiliary cell functions, the second-order auxiliary cell functions are evaluated by solving second-order auxiliary cell problems (2.23)-(2.32) with given material properties on  $V_{h_1}(Y^s)$  respectively, which correspond to different macroscopic parameters  $\bar{T}_s$ .

### 3.2. On-line computation for macroscopic homogenized problem and statistical higher-order multi-scale solutions

- (1) Define the homogenized macroscopic region  $\Omega$  in  $\mathbb{R}^N$  and partition  $Y^s$  into finite element meshes  $J^{h_0} = \{e\}$  where  $h_0 = \max_e \{h_e\}$ . Then, define the linear conforming finite element spaces  $V_{h_0}(\Omega) = \{\nu \in C^0(\bar{\Omega}) : \nu|_{\partial\Omega_T} = 0, \nu|_e \in P_1(e)\} \subset H^1(\Omega)$  and  $V_{h_0}^*(\Omega) = \{\nu \in C^0(\bar{\Omega}) : \nu|_{\partial\Omega_u} = 0, \nu|_e \in P_1(e)\} \subset H^1(\Omega)$  for simulating temperature and displacement fields, respectively.
- (2) Evaluate macroscopic homogenized material parameters on each nodes of  $V_{h_0}(\Omega)$  and  $V_{h_0}^*(\Omega)$  by interpolation method. After that, simulate the macroscopic homogenized problem (2.18) by coupled FDM-FEM method in a coarse mesh and with a large time step on the whole domain  $\Omega \times (0, T^*)$ . Employing the uniform time step  $\Delta t = T^*/M$  to discretize time-domain  $(0, T^*)$  as  $0 = t_0 < t_1 < \dots < t_M = T^*$  and  $t_N = N\Delta t$  ( $N = 0, \dots, M$ ), then we define  $f_i^N = f_i(\mathbf{x}, t_N)$ . In order to preserve the unconditional stability of our multi-scale numerical algorithm, the implicit FDM scheme is adopted in time domain and FEM scheme is employed in spatial domain. The detailed FDM-FEM scheme for macroscopic homogenized problem (2.18) is presented as below

$$\begin{cases} \int_{\Omega} \hat{S}(T_0^{N+1}) \frac{T_0^{N+1} - T_0^N}{\Delta t} \tilde{\varphi}^{h_0} d\Omega + \int_{\Omega} \hat{k}_{ij}(T_0^{N+1}) \frac{\partial T_0^{N+1}}{\partial x_j} \frac{\partial \tilde{\varphi}^{h_0}}{\partial x_i} d\Omega \\ = \int_{\Omega} h^{N+1} \tilde{\varphi}^{h_0} d\Omega + \int_{\partial\Omega_q} \bar{q}^{N+1} \tilde{\varphi}^{h_0} ds, \quad \forall \tilde{\varphi}^{h_0} \in V_{h_0}(\Omega), \\ T_0^N = \hat{T}(\mathbf{x}, t_N), \quad \text{on } \partial\Omega_T. \end{cases} \quad (3.43)$$

$$\begin{cases} \int_{\Omega} \hat{C}_{ijkl}(T_0^{N+1}) \frac{\partial u_{k0}^{N+1}}{\partial x_l} \frac{\partial \nu_i^{h_0}}{\partial x_j} d\Omega - \int_{\Omega} \hat{\beta}_{ij}(T_0^{N+1}) (T_0^{N+1} - \tilde{T}) \frac{\partial \nu_i^{h_0}}{\partial x_j} d\Omega \\ = \int_{\Omega} f_i^{N+1} \nu_i^{h_0} d\Omega + \int_{\partial\Omega_{\sigma}} \bar{\sigma}_i^{N+1} \nu_i^{h_0} ds, \quad \forall \nu^{h_0} \in (V_{h_0}^*(\Omega))^N, \\ \mathbf{u}_0^N = \hat{\mathbf{u}}(\mathbf{x}, t_N), \quad \text{on } \partial\Omega_u, \end{cases} \quad (3.44)$$

As a result, we can solve the macroscopic temperature and displacement fields at each time step via (3.43) and (3.44) by turn.

- (3) It should be highlighted that, decoupled thermal equation (3.43) is a nonlinear system which can not be computed directly. Herein, the following direct iterative method is presented for simulating the nonlinear system (3.43).

Step 1: Let  $\check{T}_0(\mathbf{x})$  be the initial function, and  $\check{T}_{\lambda}(\mathbf{x})$  be the solution at  $\lambda$ -th iterative step,  $\lambda \geq 1$ . Set the iteration threshold as  $E_{tol}$ , and begin iterating.

Step 2: At the  $\lambda$ -th iteration step, apply  $\check{T}_{\lambda-1}(\mathbf{x})$  to linearize the nonlinear system (3.43) as follows.

$$\begin{cases} \int_{\Omega} \widehat{S}(\check{T}_{\lambda-1}) \frac{\check{T}_{\lambda} - T_0^N}{\Delta t} \check{\varphi}^{h_0} d\Omega + \int_{\Omega} \widehat{k}_{ij}(\check{T}_{\lambda-1}) \frac{\partial \check{T}_{\lambda}}{\partial x_j} \frac{\partial \check{\varphi}^{h_0}}{\partial x_i} d\Omega \\ = \int_{\Omega} h^{N+1} \check{\varphi}^{h_0} d\Omega + \int_{\partial\Omega_q} \bar{q}^{N+1} \check{\varphi}^{h_0} ds, \quad \forall \check{\varphi}^{h_0} \in V_{h_0}(\Omega), \\ T_0^N = \widehat{T}(\mathbf{x}, t_N), \quad \text{on } \partial\Omega_T. \end{cases} \quad (3.45)$$

Step 3: If  $\|\check{T}_{\lambda}(\mathbf{x}) - \check{T}_{\lambda-1}(\mathbf{x})\|_{L^{\infty}(\Omega)} \leq E_{tol}$ , stop; otherwise  $\lambda = \lambda + 1$ , go back to Step 2.

Step 4: Set  $T_0^{N+1} = T_{sat}$ , where  $T_{sat}$  is the solution of linear system (3.45) which satisfies the iteration threshold as  $E_{tol}$ .

Next, substitute the obtained temperature field  $T_0^{N+1}$  into mechanical equation (3.44) and solve equation (3.44) to obtain displacement field  $\mathbf{u}_0^{N+1}$ .

- (4) For arbitrary point  $(\mathbf{x}, t) \in \Omega \times (0, T^*)$ , we apply the interpolation method to acquire the corresponding values of first-order auxiliary cell functions, second-order auxiliary cell functions and homogenized solutions. The spatial derivatives  $\frac{\partial u_{m0}}{\partial x_{\alpha_1}}$ ,  $\frac{\partial^2 u_{m0}}{\partial x_{\alpha_1} \partial x_{\alpha_2}}$ ,  $\frac{\partial T_0}{\partial x_{\alpha_1}}$  and  $\frac{\partial^2 T_0}{\partial x_{\alpha_1} \partial x_{\alpha_2}}$  in formulas (2.33) and (2.34)

are evaluated by the average technique on relative elements [43, 44], and the temporal derivatives  $\frac{\partial T_0}{\partial t}$  in formula (2.33) are evaluated by using the difference scheme (3.43) at every time steps. Then, the displacement field  $\mathbf{u}^{(2\varepsilon)}(\mathbf{x}, t)$  and temperature field  $T^{(2\varepsilon)}(\mathbf{x}, t)$  can be computed by the formulas (2.33) and (2.34). Moreover, we can further employ the higher-order interpolation method and post-processing technique in [45, 46] to obtain the high-accuracy SOTS solutions.

#### 4. Numerical experiments

In this section, the numerical accuracy and computational efficiency of the proposed SHOMS method are demonstrated by several numerical examples. Since obtaining the exact solutions for the multi-scale nonlinear problem (2.1) is extremely difficult or even impossible, direct numerical simulation (DNS) solutions on the fine grid for the multi-scale nonlinear problem (2.1) are taken as the reference solutions denoted as  $\mathbf{u}_{DNS}(\mathbf{x}, t)$  and  $T_{DNS}(\mathbf{x}, t)$ . In the following numerical experiments, some error notations are introduced as follows.

$$\text{Terr0} = \frac{\|T_0 - T_{DNS}\|_{L^2(\Omega)}}{\|T_{DNS}\|_{L^2(\Omega)}}, \quad \text{Terr1} = \frac{\|T^{(1\varepsilon)} - T_{DNS}\|_{L^2(\Omega)}}{\|T_{DNS}\|_{L^2(\Omega)}}, \quad \text{Terr2} = \frac{\|T^{(2\varepsilon)} - T_{DNS}\|_{L^2(\Omega)}}{\|T_{DNS}\|_{L^2(\Omega)}}. \quad (4.46)$$

$$\text{TErr0} = \frac{|T_0 - T_{DNS}|_{H^1(\Omega)}}{|T_{DNS}|_{H^1(\Omega)}}, \quad \text{TErr1} = \frac{|T^{(1\varepsilon)} - T_{DNS}|_{H^1(\Omega)}}{|T_{DNS}|_{H^1(\Omega)}}, \quad \text{TErr2} = \frac{|T^{(2\varepsilon)} - T_{DNS}|_{H^1(\Omega)}}{|T_{DNS}|_{H^1(\Omega)}}. \quad (4.47)$$

$$\text{Uerr0} = \frac{\|\mathbf{u}_0 - \mathbf{u}_{DNS}\|_{L^2(\Omega)}}{\|\mathbf{u}_{DNS}\|_{L^2(\Omega)}}, \quad \text{Uerr1} = \frac{\|\mathbf{u}^{(1\varepsilon)} - \mathbf{u}_{DNS}\|_{L^2(\Omega)}}{\|\mathbf{u}_{DNS}\|_{L^2(\Omega)}}, \quad \text{Uerr2} = \frac{\|\mathbf{u}^{(2\varepsilon)} - \mathbf{u}_{DNS}\|_{L^2(\Omega)}}{\|\mathbf{u}_{DNS}\|_{L^2(\Omega)}}. \quad (4.48)$$

$$\text{UErr0} = \frac{|\mathbf{u}_0 - \mathbf{u}_{DNS}|_{H^1(\Omega)}}{|\mathbf{u}_{DNS}|_{H^1(\Omega)}}, \quad \text{UErr1} = \frac{|\mathbf{u}^{(1\varepsilon)} - \mathbf{u}_{DNS}|_{H^1(\Omega)}}{|\mathbf{u}_{DNS}|_{H^1(\Omega)}}, \quad \text{UErr2} = \frac{|\mathbf{u}^{(2\varepsilon)} - \mathbf{u}_{DNS}|_{H^1(\Omega)}}{|\mathbf{u}_{DNS}|_{H^1(\Omega)}}. \quad (4.49)$$

In the above formulas,  $|\mathbf{u}_0 - \mathbf{u}_{DNS}|_{H^1(\Omega)} = \left( \sum_{i,j=1}^N \|\varepsilon_{ij}(\mathbf{u}_0 - \mathbf{u}_{DNS})\|_{L^2(\Omega)} \right)^{\frac{1}{2}}$ , where the symbol  $\varepsilon_{ij}$  represents the strain operator.

##### 4.1. Example 1: Validation of the SHOMS method for nonlinear thermo-mechanical simulation in periodic composite structure

A 2D composite structure with periodically microscopic configurations is investigated here, whose macrostructure  $\Omega$  and unit cell  $\Theta$  are shown in Fig. 3, where  $\Omega = (x_1, x_2) = [0, 1] \times [0, 1] \text{cm}^2$  and periodic unit cell size  $\varepsilon = 1/5$ . This 2D composite structure is clamped on its four side surfaces, and the temperature at the

side surfaces is kept at  $373.15K$ . In addition, we set internal heat source  $h = 5000J/(cm^2 \cdot s)$  and body forces  $(f_1, f_2) = (-2000, -2000)N/cm^2$ . Furthermore, the material parameters of 2D composite structure are demonstrated in Table 1.

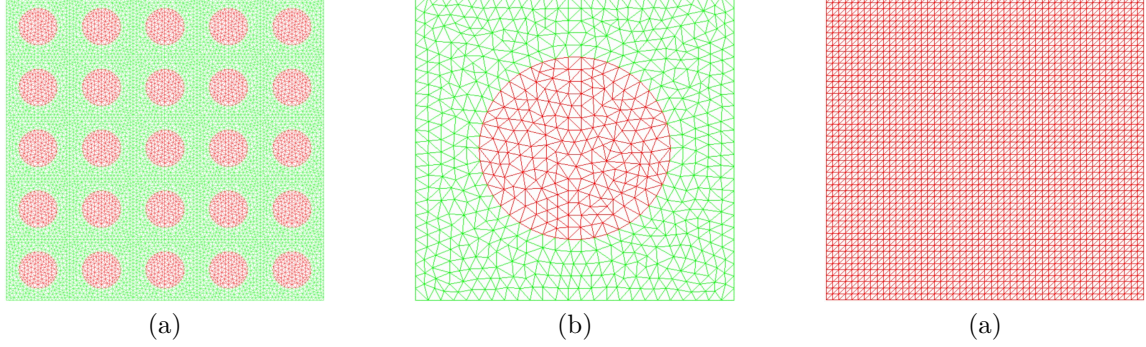


**Figure 3:** The illustration of investigated 2D composite structure: (a) FEM mesh of composite structure; (b) FEM mesh of microscopic unit cell; (c) FEM mesh of macroscopic homogenized structure.

**Table 1:** Material parameters of 2D composite structure.

Material parameters	Matrix	Inclusion
$\rho^\varepsilon$ ( $kg/m^3$ )	3210	1760
$c^\varepsilon$ ( $J/(kg \cdot K)$ )	$660.0 + 1.915T - 1.491 \times 10^{-3}T^2$	$710.0 + 1.781T - 1.976 \times 10^{-3}T^2$
$k_{ij}^\varepsilon$ ( $W/(m \cdot K)$ )	$250.0 + 0.02728T$	$8.0 + 0.02535T$
$E^\varepsilon$ ( $GPa$ )	$350.0 - 3.04 \times 10^{-2}T$	$220.0 - 1.10 \times 10^{-4}T$
$\nu^\varepsilon$	0.25	0.20
$\beta_{ij}^\varepsilon$ ( $Pa/K$ )	3.50	$9273.0 - 57.53 \times T + 0.0817 \times T^2$

Implementing the SHOMS method to multi-scale nonlinear coupling equations (2.1) in time interval  $t = [0, 1]s$  with temporal step  $\Delta t = 0.002s$ , we define service temperature range  $[273.15, 873.15]K$  of investigated composite structure and 60 representative macroscopic parameters  $\bar{T}_s$  in service temperature range. In this example, the total auxiliary cell problems need to be solved off-line 4380 times, in which the 13 first-order cell functions and 60 second-order cell functions are solved on 60 macroscopic temperature interpolation points. The information of FEM meshes is listed in Table 2. After off-line computation for microscopic cell problems and on-line computation for macroscopic homogenized problems and higher-order multi-scale solutions, we depict the computational results in Figs. 4-8.

**Table 2:** Summary of computational cost.

	Multi-scale equations.	Cell equations.	Homogenized equations.
FEM elements	17700	1370	5000
FEM nodes	9031	736	2601

According to the computational resource cost in Table 2, the presented SHOMS method can greatly economize computer memory without losing precision. Actually, both the SHOMS method and direct numerical simulation are performed on a HP desktop workstation equipped with an Intel(R) Core(TM) i7-8750H processor (2.20 GHz) and 16.0 GB of internal memory. As illustrated in Figs. 4-7, we can conclude that the higher-order multi-scale solutions can accurately capture the microscopic oscillatory behaviors and preferably approximate the exact solutions of the investigated 2D composite structure compared with macroscopic

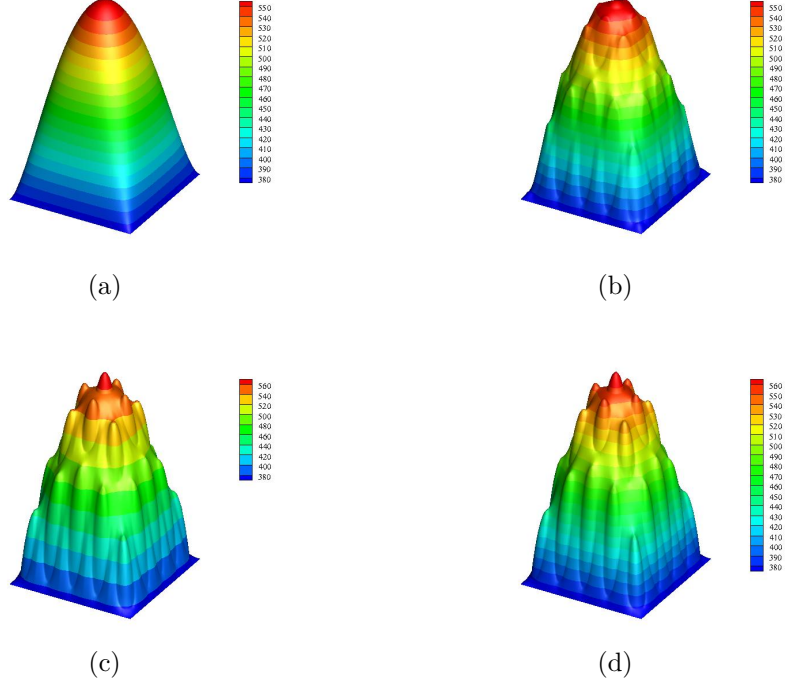


**Figure 4:** The numerical results of temperature field at  $t = 0.2s$ : (a)  $T_0$ ; (b)  $T^{(1\epsilon)}$ ; (c)  $T^{(2\epsilon)}$ ; (d)  $T_{\text{DNS}}$ .

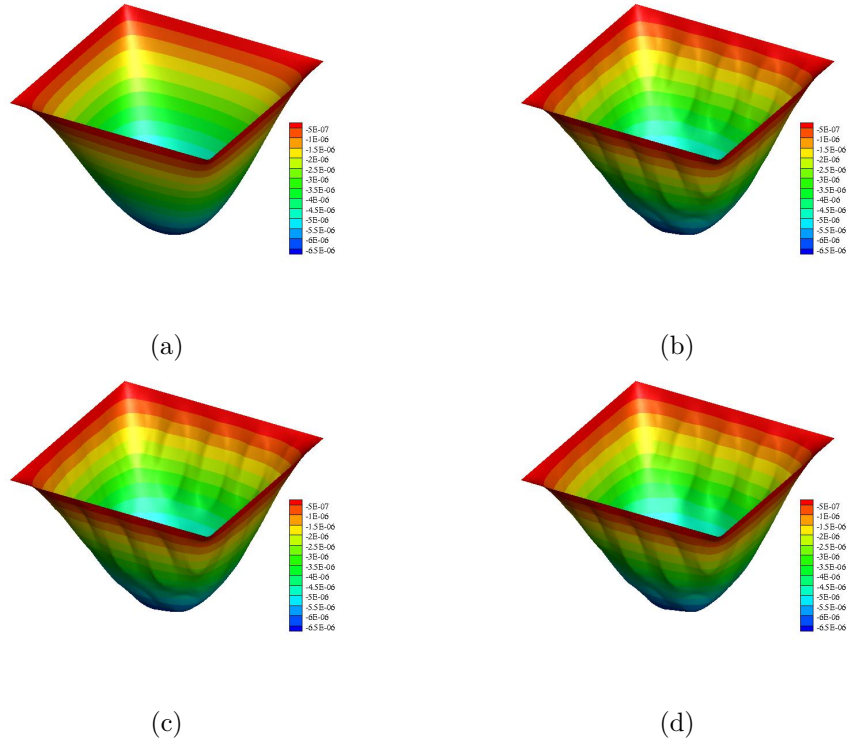


**Figure 5:** The numerical results of temperature field at  $t = 0.2s$ : (a)  $u_{10}$ ; (b)  $u_1^{(1\epsilon)}$ ; (c)  $u_1^{(2\epsilon)}$ ; (d)  $u_{1\text{DNS}}$ .

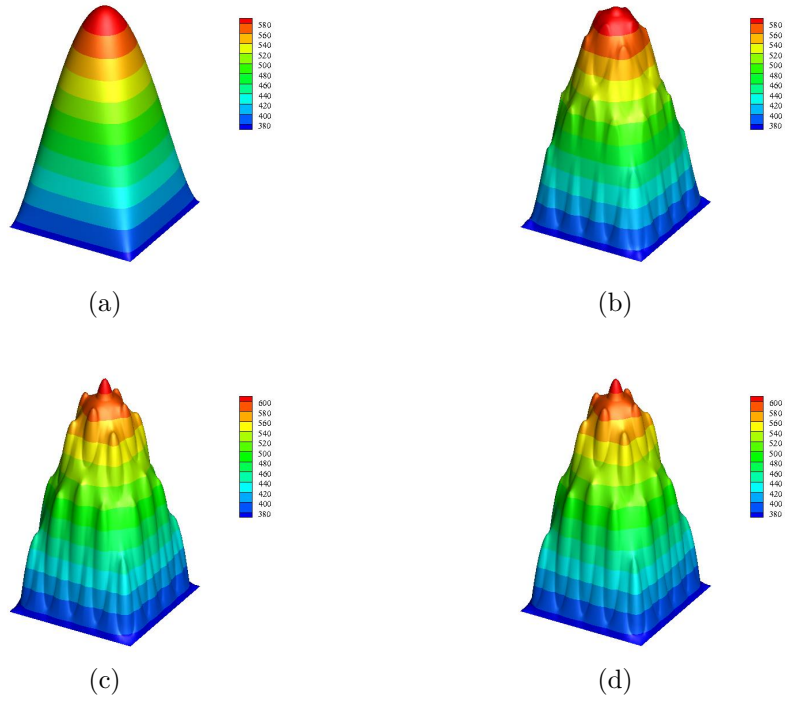


**Figure 6:** The numerical results of temperature field at  $t = 1.0s$ : (a)  $T_0$ ; (b)  $T^{(1\epsilon)}$ ; (c)  $T^{(2\epsilon)}$ ; (d)  $T_{DNS}$ .

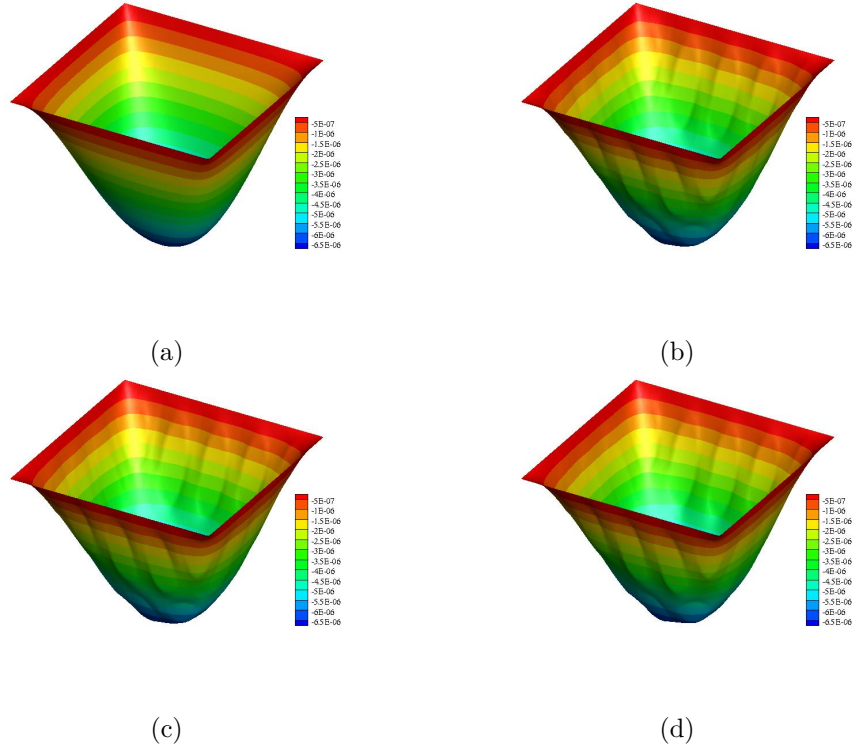


**Figure 7:** The numerical results of temperature field at  $t = 1.0s$ : (a)  $u_{10}$ ; (b)  $u_1^{(1\epsilon)}$ ; (c)  $u_1^{(2\epsilon)}$ ; (d)  $u_{1DNS}$ .

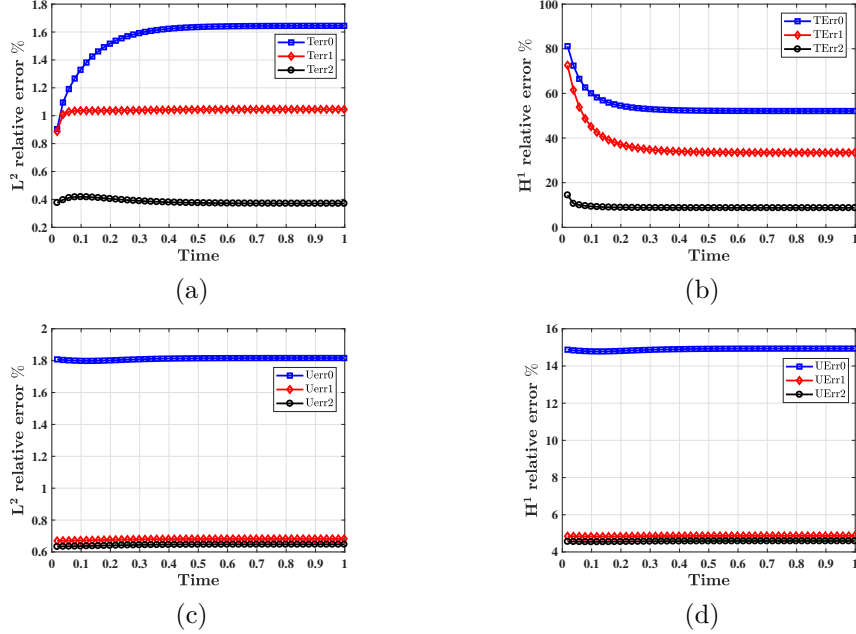


**Figure 8:** The evolutive relative errors of temperature and displacement fields: (a) Terr; (b) TErr; (c) Uerr; (d) UErr.

homogenized solutions and lower-order multi-scale solutions, especially for temperature field. From the evolutive relative errors in Fig. 8, it can clearly demonstrate that the two-stages space-time multi-scale numerical algorithm is accurate and stable in the long-time numerical simulation. Furthermore, it is worth emphasizing that the presented SHOMS approach remains effective even for a relatively small parameter  $\varepsilon$ , namely existing a great number of microscopic unit cells in inhomogeneous structures. At this time, the high-resolution DNS simulation can not guarantee the convergence for the investigated large-scale problems. This obvious advantage of the SHOMS approach is of great application values for engineering computation.

#### 4.2. Example 2: Application of the SHOMS method for equivalent material parameters computation of random composite structure

In this example, two kinds of composite materials with matrix Ti-6Al-4V and random inclusion  $\text{ZrO}_2$ , and matrix SiC and random inclusion C are investigated by the SHOMS method, as exhibited in Figs. 9. The detailed material parameters for the investigated composite materials are presented in the following Tables 3 and 4.

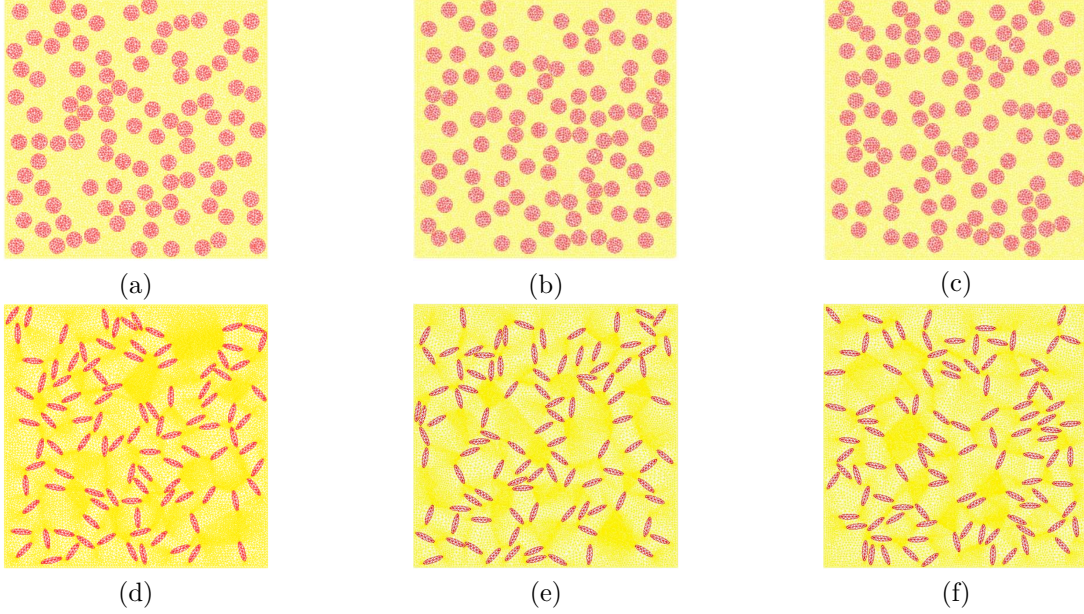
**Table 3:** Material property parameters of Ti-6Al-4V/ $\text{ZrO}_2$  composite.

Material properties	Matrix Ti-6Al-4V	Inclusion $\text{ZrO}_2$
$k_{ij}^\varepsilon$ ( $W/(m \cdot K)$ )	$1.10+0.017T$	$1.71+2.1 \times 10^{-4}T+1.16 \times 10^{-7}T^2$
$E^\varepsilon$ (GPa)	$122.7-5.65 \times 10^{-3}T$	$132.2-50.3 \times 10^{-3}T-8.1 \times 10^{-6}T^2$
$\nu^\varepsilon$	0.289	0.333

By using the SHOMS method, the equivalent material parameters at macro-scale are obtained by the mean value of 50 randomly microscopic samples. The corresponding results are depicted in Fig. 10. According to the numerical results in Fig. 10, we can conclude that the predictive values of Ti-6Al-4V/ $\text{ZrO}_2$  composite and SiC/C composite fall between lower and upper bounds of Voigt-Reuss method, Hashin-Shtrikman method and also approximate the predicted values of Hobbs method. Hence, the proposed SHOMS can be employed to predict the temperature-dependent equivalent material properties of Ti-6Al-4V/ $\text{ZrO}_2$  composite and SiC/C composite.

**Table 4:** Material property parameters of SiC/C composite.

Material properties	Matrix SiC	Inclusion C
$k_{ij}^\varepsilon$ ( $W/(m \cdot K)$ )	250.0+0.02728 $T$	8.0+0.02535 $T$
$E^\varepsilon$ (GPa)	350.0-3.04 $\times 10^{-2}T$	220.0-1.10 $\times 10^{-4}T$
$\nu^\varepsilon$	0.25	0.20

**Figure 9:** Several random RVEs of the composites employed for predicting equivalent material parameters: (a)-(c) particulate composites with volume fraction 28.2743%; (d)-(f) fibrous composites with volume fraction 12.5664%.

#### 4.3. Example 3: Application of the SHOMS method for nonlinear thermo-mechanical simulation in random composite structure

This example study the nonlinear thermo-mechanical simulation of 2D composite structure with randomly microscopic configurations, as depicted in Fig. 11. In addition, the setting of initial-boundary conditions, heat source, body forces and material parameters in this example is the same as those of Example 1.

Applying the SHOMS method to multi-scale nonlinear coupling equations (2.1) within time interval  $t = [0, 1]s$  with temporal step  $\Delta t = 0.002s$ , we establish the service temperature range of the investigated composite structure as  $[273.15, 873.15]K$ . In this service temperature range, we distribute 60 representative macroscopic parameters  $\bar{T}_s$ . The detailed information of FEM meshes is listed in Table 5. After off-line computation for microscopic cell problems and on-line computation for macroscopic homogenized problems and higher-order multi-scale solutions, we present the computational results in Figs. 12-16.

**Table 5:** Summary of computational cost.

	Multi-scale equations.	Cell equations.	Homogenized equations.
FEM elements	33800	1352	5000
FEM nodes	17151	727	2601

As indicated Table 5, the presented SHOMS method can significant reduce computer memory without losing precision. Moreover, the numerical results in Figs. 12-15 reveal that the higher-order multi-scale solutions can accurately capture the microscopic oscillatory behaviors and provide preferable approximations

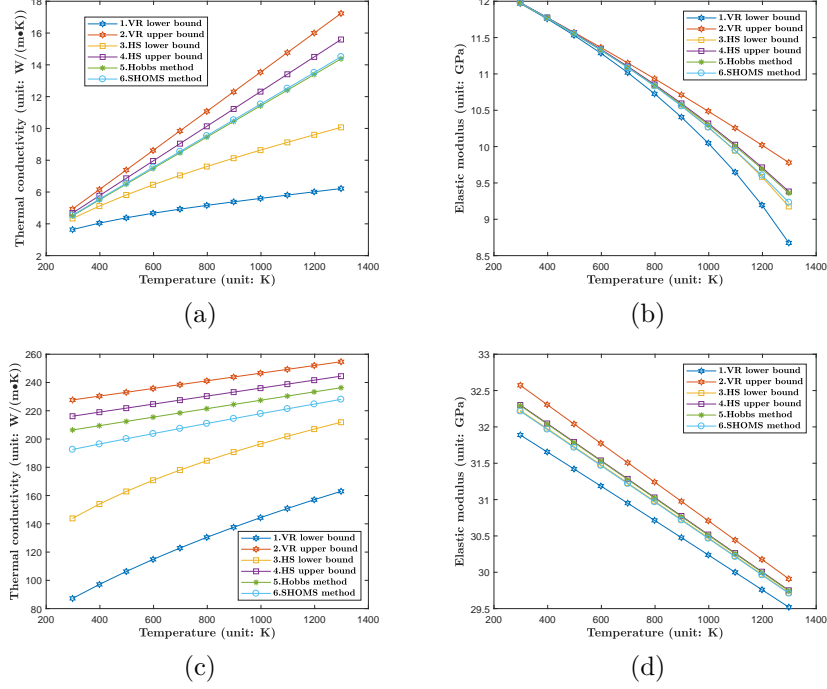


**Figure 10:** A comparison of the predictive results of equivalent material parameters: (a) nonlinear elastic modulus of particulate composites; (b) nonlinear thermal conductivity of particulate composites; (c) nonlinear elastic modulus of fibrous composites; (d) nonlinear thermal conductivity of fibrous composites.

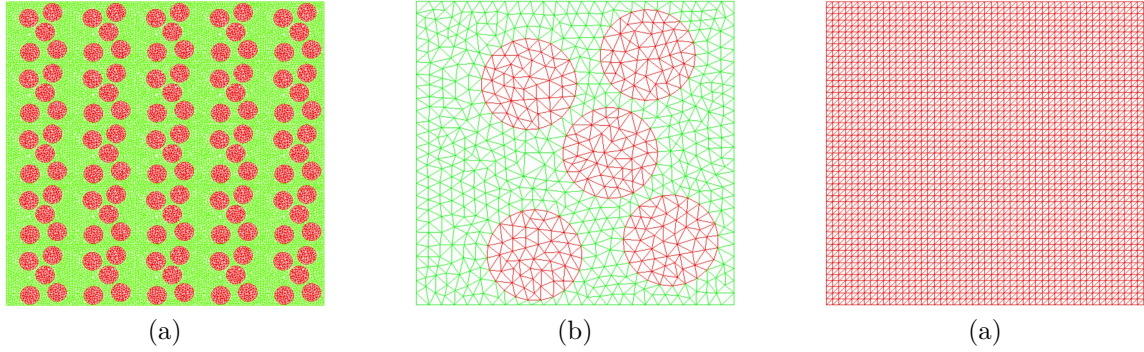


**Figure 11:** The illustration of investigated 2D composite structure: (a) FEM mesh of composite structure; (b) FEM mesh of microscopic unit cell; (c) FEM mesh of macroscopic homogenized structure.

to the exact solutions of the investigated 2D composite structure compared with macroscopic homogenized solutions and lower-order multi-scale solutions, especially for temperature field. The evolutive relative errors shown in Fig. 16 clearly demonstrate the accuracy and stability of the two-stages space-time multi-scale numerical algorithm in the long-time numerical simulation. Furthermore, it is important to highlight that the presented SHOMS approach remains effective even for a relatively small parameter  $\varepsilon$ , which corresponds to a large number of microscopic unit cells in inhomogeneous structures. In contrast, the high-resolution DNS simulation fails to converge for the investigated large-scale problems. This prominent computational advantage of the proposed SHOMS framework is of significant practical value of the SHOMS approach in engineering computations.

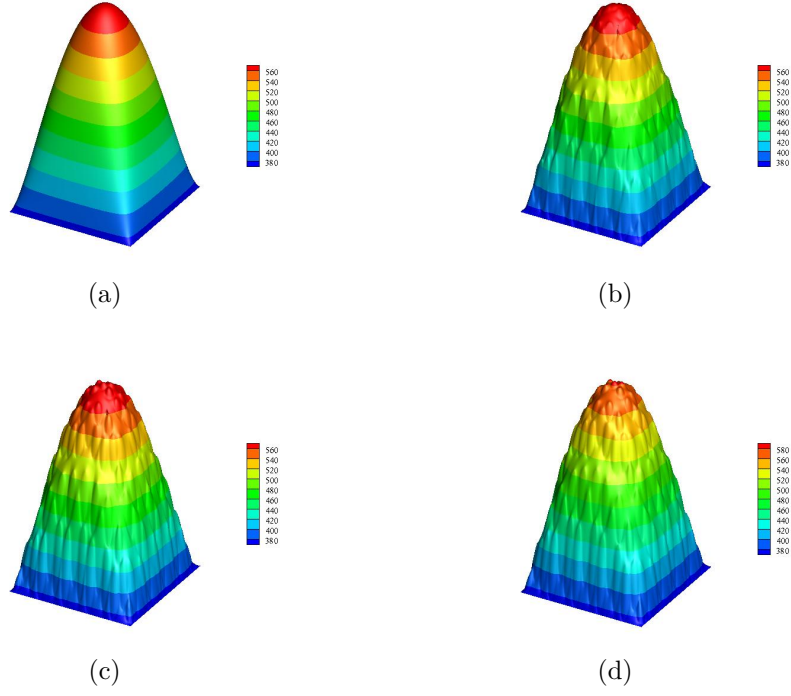


**Figure 12:** The numerical results of temperature field at  $t = 0.2s$ : (a)  $T_0$ ; (b)  $T^{(1\varepsilon)}$ ; (c)  $T^{(2\varepsilon)}$ ; (d)  $T_{DNS}$ .

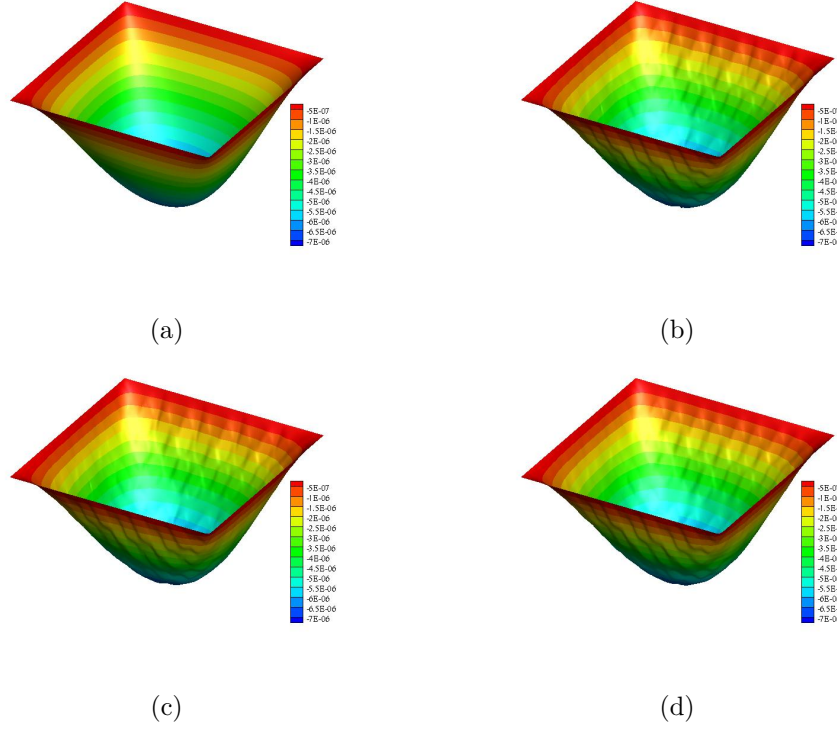


**Figure 13:** The numerical results of temperature field at  $t = 0.2s$ : (a)  $u_{10}$ ; (b)  $u_1^{(1\varepsilon)}$ ; (c)  $u_1^{(2\varepsilon)}$ ; (d)  $u_{1DNS}$ .

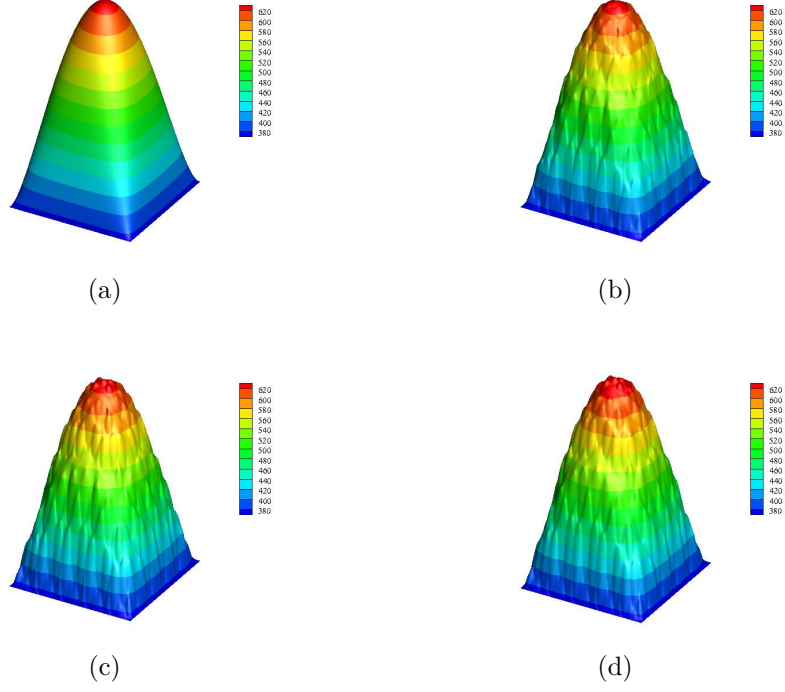


**Figure 14:** The numerical results of temperature field at  $t = 1.0s$ : (a)  $T_0$ ; (b)  $T^{(1\varepsilon)}$ ; (c)  $T^{(2\varepsilon)}$ ; (d)  $T_{DNS}$ .

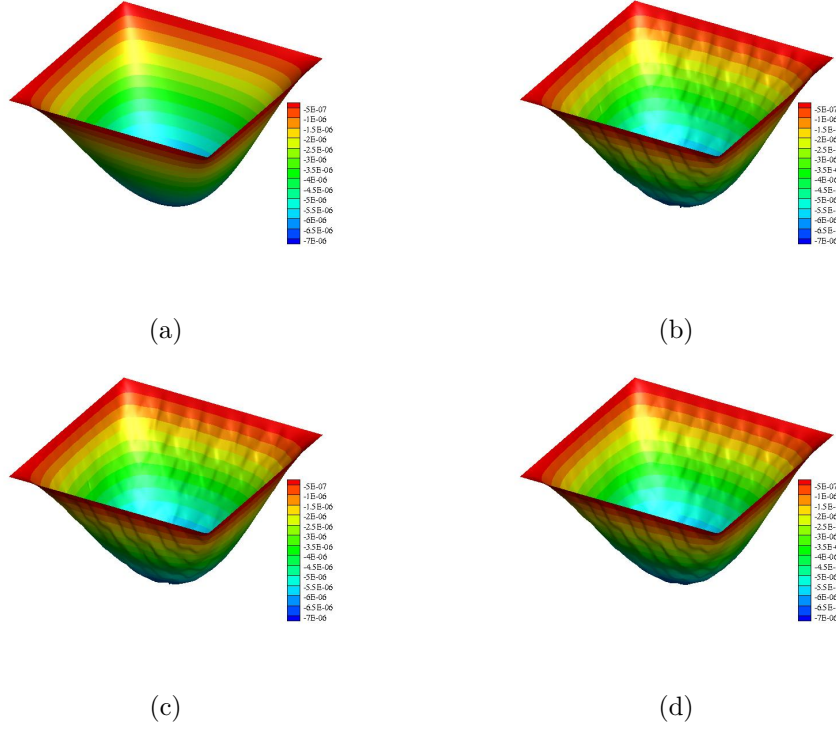


**Figure 15:** The numerical results of temperature field at  $t = 1.0s$ : (a)  $u_{10}$ ; (b)  $u_1^{(1\varepsilon)}$ ; (c)  $u_1^{(2\varepsilon)}$ ; (d)  $u_{1DNS}$ .

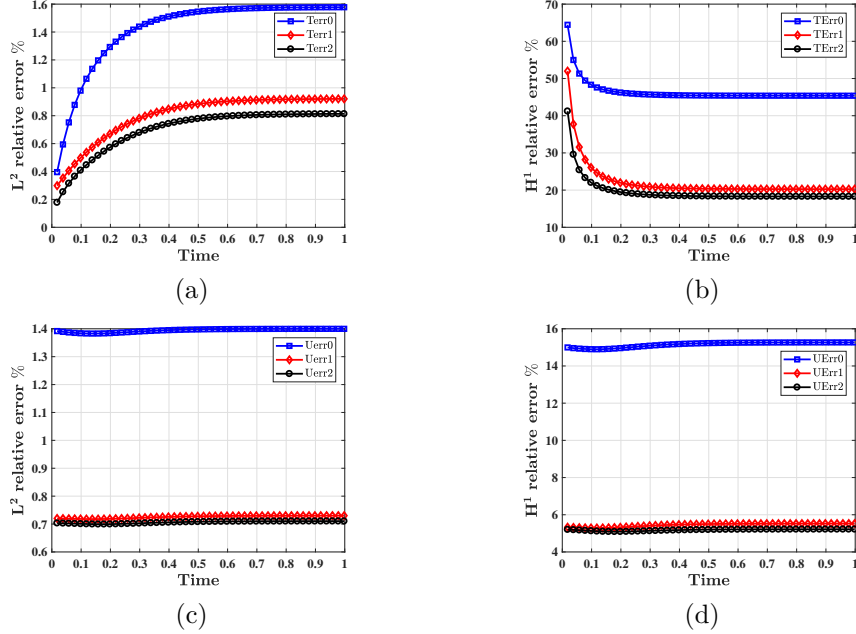


**Figure 16:** The evolutive relative errors of temperature and displacement fields: (a) TErr; (b) TErr; (c) Uerr; (d) UErr.

## 5. Conclusions and outlook

In the present work, a novel statistical higher-order multi-scale method is developed with the aim of effectively simulating nonlinear thermo-mechanical simulation of random composite materials with temperature-dependent properties, which served under extreme heat environment. The main contributions of this work are threefold: First, the statistical multi-scale formulations with the higher-order correction terms are established for random composites under statistical periodic configurations. Second, the local error estimations for the statistical multi-scale solutions of nonlinear thermo-mechanical systems are derived in detail. Third, a space-time numerical algorithm with off-line and on-line stages is designed to overcome the prohibitive computation of direct numerical simulation. Furthermore, numerical results demonstrate that the presented SHOMS approach can effectively simulate nonlinear thermo-mechanical coupling behaviors with less computational cost and accurately capture the microscopic oscillatory information caused by randomly heterogeneous configurations. Besides, the proposed SHOMS approach can accurately predict the equivalent material parameters of random composites compared with the predictive results of some theoretical models, which illustrate that high temperature field has a remarkable effect on macroscopic thermo-mechanical properties.

In the future, the SHOMS method will be extended to more complex nonlinear problems including thermal convection and radiation effects under extreme thermal environment. Additionally, machine learning approaches and parallel algorithm will be introduced in the off-line stage of SHOMS framework, in order to avoid repetitive statistical computation and improve computational efficiency.

## Acknowledgments

The authors gratefully acknowledge the support of the the National Natural Science Foundation of China (Nos. 12001414 and 51739007), Young Talent Fund of Association for Science and Technology in Shaanxi, China (No. 20220506), Young Talent Fund of Association for Science and Technology in Xi'an, China (No. 095920221338), the Fundamental Research Funds for the Central Universities (No. KYFZ23020).

## References

## References

- [1] T. Skinner, A. Chattopadhyay, Multiscale temperature-dependent ceramic matrix composite damage model with thermal residual stresses and manufacturing-induced damage, *Composite Structures* 268 (2021) 114006.
- [2] Z. Li, Y. Wang, X. Sun, L. Guo, L. Zhang, Honeycomb-based method for generating random fiber distributions of fiber reinforced composites and transverse mechanical properties prediction, *Composite Structures* 266 (2021) 113794.
- [3] H. Zhang, D. Yang, S. Zhang, Y. Zheng, Multiscale nonlinear thermoelastic analysis of heterogeneous multiphase materials with temperature-dependent properties, *Finite Elements in Analysis and Design* 88 (2014) 97–117.
- [4] J. N. Reddy, C. D. Chin, Thermomechanical analysis of functionally graded cylinders and plates, *Journal of Thermal Stresses* 21 (1998) 593–626.
- [5] M. Shariyat, M. Khaghani, S. M. H. Lavasani, Nonlinear thermoelasticity, vibration, and stress wave propagation analyses of thick fgm cylinders with temperature-dependent material properties, *European Journal of Mechanics A-solids* 29 (2010) 378–391.
- [6] T. Matsumoto, A. Guzik, M. Tanaka, A boundary element method for analysis of thermoelastic deformations in materials with temperature dependent properties, *International Journal for Numerical Methods in Engineering* 64 (2005) 1432–1458.
- [7] A. J. Goupee, S. S. Vel, Multi-objective optimization of functionally graded materials with temperature-dependent material properties, *Materials & Design* 28 (2007) 1861–1879.
- [8] F. Abdoun, L. Azrar, Thermal buckling and vibration of laminated composite plates with temperature dependent properties by an asymptotic numerical method, *International Journal for Computational Methods in Engineering Science and Mechanics* 21 (2020) 43–57.
- [9] A. Najibi, P. Alizadeh, P. Ghazifard, Transient thermal stress analysis for a short thick hollow fgm cylinder with nonlinear temperature-dependent material properties, *Journal of Thermal Analysis and Calorimetry* (2021) 1–12.
- [10] Z. Zhang, D. Zhou, X. Xu, X. Li, Analysis of thick beams with temperature-dependent material properties under thermomechanical loads, *Advances in Structural Engineering* 23 (2020) 1838–1850.
- [11] A. Bensoussan, J.-L. Lions, G. Papanicolaou, *Asymptotic analysis for periodic structures*, American Mathematical Soc., 2011.
- [12] T. Hou, X. H. Wu, Z. Cai, Convergence of a multiscale finite element method for elliptic problems with rapidly oscillating coefficients, *Mathematics of Computation* 68 (1999) 913–943.
- [13] W. E, P. Ming, P. Zhang, Analysis of the heterogeneous multiscale method for elliptic homogenization problems, *Journal of the American Mathematical Society* 18 (2005) 121–156.
- [14] T. J. Hughes, G. R. Feijóo, L. Mazzei, J. B. Quincy, The variational multiscale method-a paradigm for computational mechanics, *Computer Methods in Applied Mechanics and Engineering* 166 (1998) 3–24.
- [15] Y. Xing, Y. Yang, X. Wang, A multiscale eigenelement method and its application to periodical composite structures, *Composite Structures* 92 (2010) 2265–2275.
- [16] P. Henning, A. Målqvist, Localized orthogonal decomposition techniques for boundary value problems, *SIAM Journal on Scientific Computing* 36 (2014) A1609–A1634.
- [17] Z. He, M.-J. Pindera, Finite volume based asymptotic homogenization theory for periodic materials under anti-plane shear, *European Journal of Mechanics-A/Solids* 85 (2021) 104122.

- [18] Y. T. Wu, Y. F. Nie, Z. H. Yang, Comparison of four multiscale methods for elliptic problems, *CMES-Computer Modeling in Engineering & Sciences* 99 (2014) 297–325.
- [19] H. Dong, Y. Nie, Z. Yang, Y. T. Wu, The Numerical Accuracy Analysis of Asymptotic Homogenization Method and Multiscale Finite Element Method for Periodic Composite Materials, *CMES-Computer Modeling in Engineering & Sciences* 111 (2016) 395–419.
- [20] Y. Gao, Y. Xing, Z. Huang, M. Li, Y. Yang, An assessment of multiscale asymptotic expansion method for linear static problems of periodic composite structures, *European Journal of Mechanics-A/Solids* 81 (2020) 103951.
- [21] X. Wang, L. Cao, Y. Wong, Multiscale computation and convergence for coupled thermoelastic system in composite materials, *Multiscale Modeling & Simulation* 13 (2015) 661–690.
- [22] X. Guan, X. Liu, X. Jia, Y. Yuan, J. Cui, H. A. Mang, A stochastic multiscale model for predicting mechanical properties of fiber reinforced concrete, *International Journal of Solids and Structures* 56 (2015) 280–289.
- [23] Z. Yang, J. Cui, The Statistical Second-Order Two-Scale Analysis for Dynamic Thermo-Mechanical Performances of the Composite Structure with Consistent Random Distribution of Particles, *Computational Materials Science* 69 (2013) 359–373.
- [24] Z. Yang, J. Cui, Y. Sun, J. Liang, Z. Yang, Multiscale analysis method for thermo-mechanical performance of periodic porous materials with interior surface radiation, *International Journal for Numerical Methods in Engineering* 105 (2016) 323–350.
- [25] Z. H. Li, Q. Ma, J. Cui, Second-order two-scale finite element algorithm for dynamic thermo-mechanical coupling problem in symmetric structure, *Journal of Computational Physics* 314 (2016) 712–748.
- [26] H. Dong, X. Zheng, J. Cui, Y. Nie, Z. Yang, Q. Ma, Multi-scale computational method for dynamic thermo-mechanical performance of heterogeneous shell structures with orthogonal periodic configurations, *Computer Methods in Applied Mechanics and Engineering* 354 (2019) 143–180.
- [27] H. Dong, J. Cui, Y. Nie, R. Ma, K. Jin, D. Huang, Multi-scale computational method for nonlinear dynamic thermo-mechanical problems of composite materials with temperature-dependent properties, *Communications in Nonlinear Science and Numerical Simulation* 118 (2023) 107000.
- [28] H. Dong, Z. Yang, X. Guan, J. Cui, Stochastic higher-order three-scale strength prediction model for composite structures with micromechanical analysis, *Journal of Computational Physics* 465 (2022) 111352.
- [29] M. Kamiński, Generalized perturbation-based stochastic finite element method in elastostatics, *Computers & structures* 85 (2007) 586–594.
- [30] M. Kamiński, M. Kleiber, Perturbation based stochastic finite element method for homogenization of two-phase elastic composites, *Computers & structures* 78 (2000) 811–826.
- [31] P. Wen, N. Takano, D. Kurita, Probabilistic multiscale analysis of three-phase composite material considering uncertainties in both physical and geometrical parameters at microscale, *Acta Mechanica* 227 (2016) 2735–2747.
- [32] R. G. Ghanem, P. D. Spanos, *Stochastic finite elements: a spectral approach*, Courier Corporation, 2003.
- [33] M. Jurdak, R. Ghanem, Spectral stochastic homogenization of divergence-type pdes, *Computer Methods in Applied Mechanics and Engineering* 193 (2004) 429–447.
- [34] M. Tootkaboni, L. Graham-Brady, A multi-scale spectral stochastic method for homogenization of multi-phase periodic composites with random material properties, *International journal for numerical methods in engineering* 83 (2010) 59–90.

- [35] D. Xiu, J. S. Hesthaven, High-order collocation methods for differential equations with random inputs, *SIAM Journal on Scientific Computing* 27 (2005) 1118–1139.
- [36] B. Ganapathysubramanian, N. Zabaras, Modeling diffusion in random heterogeneous media: Data-driven models, stochastic collocation and the variational multiscale method, *Journal of Computational Physics* 226 (2007) 326–353.
- [37] Z. Yang, Y. Sun, Y. Liu, J. Cui, Prediction on nonlinear mechanical performance of random particulate composites by a statistical second-order reduced multiscale approach, *Acta Mechanica Sinica* 37 (2021) 570–588.
- [38] Z. Yang, J. Cui, Y. Sun, Y. Liu, Y. Xiao, A stochastic multiscale method for thermo-mechanical analysis arising from random porous materials with interior surface radiation, *Advances in Engineering Software* 104 (2017) 12–27.
- [39] Z. Yang, X. Guan, J. Cui, H. Dong, Y. Wu, J. Zhang, Stochastic multiscale heat transfer analysis of heterogeneous materials with multiple random configurations, *Commun. Comput. Phys* 27 (2020) 431–459.
- [40] Y. Li, J. Cui, Two-scale analysis method for predicting heat transfer performance of composite materials with random grain distribution, *Science in China Series A: Mathematics* 47 (2004) 101–110.
- [41] H. Dong, J. Linghu, Y. Nie, Integrated wavelet-learning method for macroscopic mechanical properties prediction of concrete composites with hierarchical random configurations, *Composite Structures* 304 (2023) 116357.
- [42] F. Hecht, *FreeFem++* (Third Edition), Version 3.60, Laboratoire Jacques-Louis Lions, Université Pierre et Marie Curie, 2015.
- [43] L.-Q. Cao, Multiscale asymptotic expansion and finite element methods for the mixed boundary value problems of second order elliptic equation in perforated domains, *Numerische Mathematik* 103 (2006) 11–45.
- [44] J. Cui, Multi-scale computational method for unified design of structure, components and their materials. invited presentation on “Chinese conference of computational mechanics, cccm-2001”, Proc. On "Computational Mechanics in Science and Engineering", Peking University Press (2001).
- [45] Q. L. Dong, L. Q. Cao, Multiscale asymptotic expansions methods and numerical algorithms for the wave equations of second order with rapidly oscillating coefficients, *Applied Numerical Mathematics* 59 (2009) 3008–3032.
- [46] Q. Lin, Q. D. Zhu, *The Preprocessing and Preprocessing for the Finite Element Method*, Shanghai Scientific & Technical Publishers, 1994.